FG.

(3)

TECHNICAL REPORT RE-75-30

ANALYSIS OF RADAR CROSS SECTION MEASUREMENTS OF A SCALE MODEL OF THE MQM-34D

James Wright
Advanced Sensors Directorate
US Army Missile Research, Development and Engineering Laboratory
US Army Missile Command
Redstone Arsenal, Alabama 35809

12 May 1975

U.S. ARMY MISSILE COMMAND
Redstone Arsenal, Alabama 35809

DISPOSITION INSTRUCTIONS

DESTROY THIS REPORT WHEN IT IS NO LONGER NEEDED. DO NOT RETURN IT TO THE ORIGINATOR.

DISCLAIMER

THE FINDINGS IN THIS REPORT ARE NOT TO BE CONSTRUED AS AN OFFICIAL DEPARTMENT OF THE ARMY POSITION UNLESS SO DESIGNATED BY OTHER AUTHORIZED DOCUMENTS.

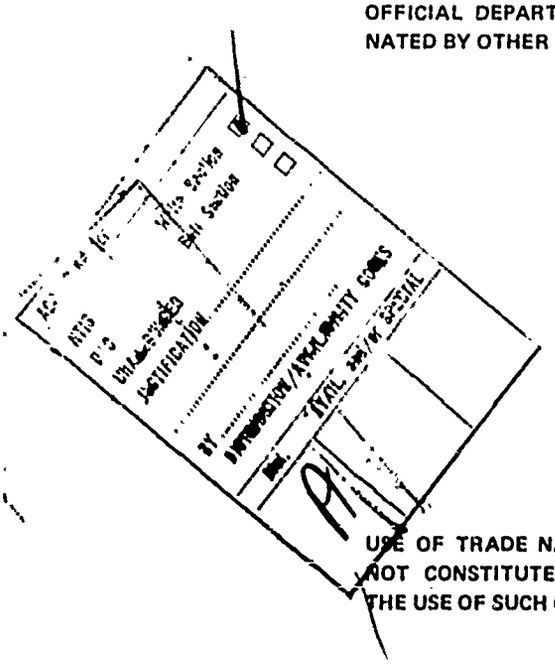

TRADE NAMES

USE OF TRADE NAMES OR MANUFACTURERS IN THIS REPORT DOES NOT CONSTITUTE AN OFFICIAL INDORSEMENT OR APPROVAL OF THE USE OF SUCH COMMERCIAL HARDWARE OR SOFTWARE.

UNCLASSIFIED

SECURITY CLASSIFICATION OF THIS PAGE *(When Data Entered)*

REPORT DOCUMENTATION PAGE	READ INSTRUCTIONS BEFORE COMPLETING FORM
1. REPORT NUMBER: RE-75-30	2. GOVT ACCESSION NO.
3. RECIPIENT'S CATALOG NUMBER	
4. TITLE *(and Subtitle)*: ANALYSIS OF RADAR CROSS SECTION MEASUREMENTS OF A SCALE MODEL OF THE MQM-34D	5. TYPE OF REPORT & PERIOD COVERED: Technical Report
6. PERFORMING ORG. REPORT NUMBER: RE-75-30	
7. AUTHOR(s): James W. Wright	8. CONTRACT OR GRANT NUMBER(s)
9. PERFORMING ORGANIZATION NAME AND ADDRESS: Commander, US Army Missile Command, ATTN: AMSMI-RE, Redstone Arsenal, Alabama 35809	10. PROGRAM ELEMENT, PROJECT, TASK AREA & WORK UNIT NUMBERS
11. CONTROLLING OFFICE NAME AND ADDRESS: Commander, US Army Missile Command, ATTN: AMSMI-RPR, Redstone Arsenal, Alabama 35809	12. REPORT DATE: 12 May 1975 13. NUMBER OF PAGES: 35
14. MONITORING AGENCY NAME & ADDRESS *(If different from Controlling Office)*: 51p.	15. SECURITY CLASS. *(of this report)*: UNCLASSIFIED 15a. DECLASSIFICATION/DOWNGRADING SCHEDULE

16. DISTRIBUTION STATEMENT *(of this Report)*

Approved for public release; distribution unlimited.

17. DISTRIBUTION STATEMENT *(of the abstract entered in Block 20, if different from Report)*

18. SUPPLEMENTARY NOTES

19. KEY WORDS *(Continue on reverse side if necessary and identify by block number)*

20. ABSTRACT *(Continue on reverse side if necessary and identify by block number)*

(U) Monostatic radar cross section (RCS) measurements of a half scale model of the MQM-34D target drone are reduced and analyzed for vertical principal circular, and cross circular polarizations. The vertically polarized measurements are also compared with RCS measurements of a full-scale drone. The RCS measurements are reduced on a cut-by-cut basis and on an aspect angle region basis. The former method is more conventional and provides insight into some details of the scattering. The second method is of interest for statistical comparisons of the different polarizations.

DD FORM 1 JAN 73 1473 EDITION OF 1 NOV 65 IS OBSOLETE

UNCLASSIFIED

SECURITY CLASSIFICATION OF THIS PAGE *(When Data Entered)*

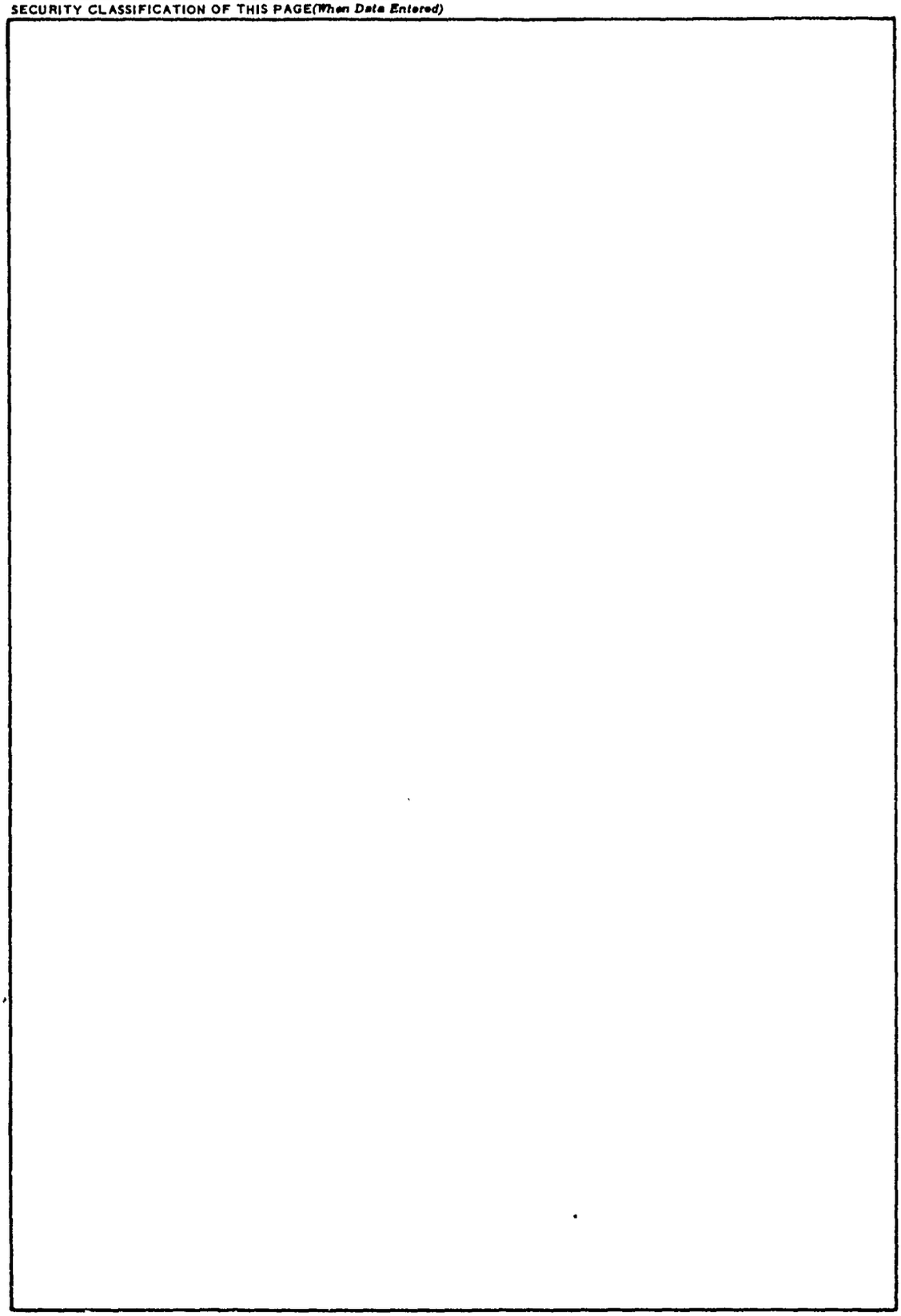

CONTENTS

1. Introduction

This report presents the results of an analysis of the characteristics of the monostatic radar cross section (RCS) of a scale model of the MQM-34D (Air Force designation/BQM-34A) target drone, also known as the FIREBEE. The data were taken by the Convair Aerospace Division, General Dynamics (GD/CAD), Fort Worth, Texas, under a contract with the Raytheon Company for the development of a discrete scatterer target model for use in simulations of the SAM-D air defense system.

The data were partially analyzed previously by GD/CAD[1] to determine the possible advantages and disadvantages of utilizing circular polarization for an all-weather radar guided missile system. The analysis presented here extends the previous analysis and compares the scale model measurements with full size target measurements.

The circular polarization RCS is approximately 1.5 dB lower than the vertical polarization data near nose-on, with the principal and cross circular polarization differing by less than 0.5 dB. In the near broadside aspect angle region where the large speculars from the fuselage and aerodynamic surfaces dominate the vertical and principal circular polarization measurements are essentially the same, and the cross circular polarization measurement is approximately 10 dB lower.

There are significant differences in the measurements on the two targets. Although the measurements were made on different ranges, the principal differences appear to be due to the differences in the targets.

2. Target Model

The target model was a 0.55 scale model of the MQM-34D, based upon drawings and data supplied by Teledyne-Ryan. The model was constructed of fiberglass and all conductive surfaces were flame sprayed or painted with a conductive aluminum coating. The model was a reasonably accurate model of the real aircraft, but differ in a number of ways.

The front cowling of the drone, from the radome to the first bulkhead, is a fiberglass structure on which no specific electromagnetic characteristics were available. For simplicity and configuration control, it was decided that the cowl should be made conductive. To further

---

[1] Clay, R. W., and Johnston, J. K., BQM-34A Polarization Characteristics-Radar Cross Section and Glint, General Dynamics Report Number FZE-1312, General Dynamics Convair Aerospace Division, Fort Worth, Texas, Contract Number DAAH01-73-C-11D2, Final Report, February 1974.

simplify the modeling, the space behind the radome mounting ring was plugged with radar absorbing material (RAM). These modifications were also made to the full size drone measured at RATSCAT.

The engine in-take duct was modeled back to the engine. The engine modeling included the engine support struts and the first stage of the compressor. This was backed by RAM to prevent reflections being reradiated from within the fuselage. The engine exhaust duct was modeled in detail but no turbine stages were modeled. The duct was terminated in RAM. (The model was only required to be accurate for aspect angles up to 120° from nose-on).

All external structures, including the riser cover, JATO thrust lug, etc., were accurately modeled in physical size and shape. Perhaps the major deviation from realism is the smooth, continuously conductive skin. The skin was not broken at the apparent discontinuities such as hatch covers, ailerons, etc. A photograph of the model is shown in Figure 1.

3. Measurement Conditions

These long pulse measurements were made on a ground plane range at a distance of 1800 feet. The target orientations for the eleven data cuts are listed in Table 1, and the corresponding aspect angles are shown in Figure 2. Three polarizations were used in the measurements:

a) Vertical transmit-vertical receive, denoted as VV.

b) Right circular transmit-left circular receive, i.e., principal circular, denoted as RL.

c) Left circular transmit-left circular receive, i.e., cross circular, denoted as LL.

The rectilinear plots of these measurements were included as Appendix A of Reference 1. The scale in those plots is in measured RCS at the actual measurement frequency. The data in this report have been corrected for the model scale factor, i.e., 5.2 dB have been added to the actual measurements.

The dynamic range of the GD/CAD measurement system is limited to 50 dB as compared to 70 dB for the RATSCAT system. Therefore, some clipping occurs in the data. The effect of the clipping is not the same on all runs. This is due to setting the system gain to take maximum advantage of the usable dynamic range. The effect is apparent in the analysis since no method was available to correct the problem. The regions of low average RCS are probably most affected, since the clipping is most apparent for the very small RCS values.

TABLE 1. ROLL AND PITCH ANGLES FOR DATA CUTS.

Pitch Angle (deg)	Roll Angle (deg)
0	0
0	20
0	90
-45	-90
-30	-90
20	0
45	0
-20	0
-45	0
-15	90
0	45

4. Data Reduction and Analysis

The data have been processed in two different ways. The first was to compute the average and standard deviation of the RCS for each cut, using a uniformly weighted 5° sliding window every 2.5°. The average and standard deviation are computed for the RCS in square meters (m^2) and the resulting values are then converted to decibels referenced to one square meter (dBm^2) for plotting. The second data reduction technique was to select all data in a specific aspect angle region for each polarization and determine the statistical characteristics of these sets of data. The probability distributions of these sets of data are then compared with three classical probability distributions for RCS. The three classical probability distributions are the Swerling 1, Swerling 3, and the log-normal. The average and standard deviation used in the Swerling models are computed in m^2 and in the log-normal model are computed in dBm^2.

It is appropriate to compare the measurements of the 0.55 scale model and the full-scale target before analyzing the model measurements. The reason for this will become apparent. Figures 3, 4, 5 and 6 are plots of the measurements for the four cuts of data which are directly comparable. The upper plot is the RCS measured at RATSCAT[2] and the lower

[2] Radar Signature Measurements of BQM-34A and BQM-34F Target Drones, AFSWC-TR-74-01, Air Force Special Weapons Center, 6585th Test Group (RX), Holloman Air Force Base, NW, January 1974.

plot is the RCS measured at GD/CAD. The GD/CAD data have been rescaled to reflect the RCS of a full-scale target.

The differences between the sets of measurements are quite noticeable. The lobing structure in the GD/CAD measurements is much lower than those in the RATSCAT measurements. In addition, there are many aspect angles for which the RCS of the scale model is significantly lower than the full-scale target. Since the RCS values are similar for the aspect angles where the large speculars from the fuselage and aerodynamic surfaces dominate, it must be concluded that the differences are caused largely by the differences between the objects measured.

The full-scale target drone measured at RATSCAT was randomly picked from the available inventory at Holloman Air Force Base, NW. It was flightworthy but did indicate considerable use through small dents, repairs, poorly fitting hatch covers and joints, etc. The 0.55 scale model, on the other hand, was a precision-built model with a very smooth continuous conductive surface. This difference is probably the main source of the difference in electromagnetic (EM) signature. Some small discrepancy in the engine and engine inlet probably exists due to the decision to model only one of the compressors. This was considered acceptable since the model was not made to be accurate more than 120° from nose-on.

The measured RCS of the 0.55 scale model looks more like a mathematical model than actual measurements. This probably should be expected because of the smooth surfaces involved. One significant aspect of this is the effect on the scattering characteristics for the circularly polarized measurements. There are many fewer edges to depolarize the incident EM field on the scale model than on the full size drone. Therefore, the cross-circular polarization data may be underestimated in the regions where multiple reflections are small.

The differences in the EM scattering must also exist on the short pulse data from which the discrete scatterer model (DSM) is derived. Since this model neglects many existing small scatterers, some discretion and judgement must be used when evaluating system performance estimation using the DSM.

These apparently negative comments should not be construed as a criticism of the contractor since other knowledgeable personnel in the field, including Government personnel, participated in many of the decisions. Even in retrospect, it is difficult to determine how the results could have been improved without considerable costly experimentation.

Figures 7 through 17 present plots of the averages and standard deviations of the RCS for the three polarizations using the uniformly

weighted 5° sliding window. The effects of polarization on the RCS are quite apparent. For example, consider Figure 7:

a) In the nose-on region, the cross-circular polarization RCS exceeds the principal circular RCS by approximately 15 dB, and exceeds the vertical polarization RCS by approximately 5 dB. The engine inlet scattering is clearly dominated by an even number of bounces.

b) In the near broadside aspects, the vertical and principal circular polarization RCS are nearly identical, and some 10 dB or more higher than the cross-circular RCS.

Similar observations can be made on the other figures. In fact, it is easier to determine where multiple reflections occur using the two sets of circularly polarized measurements than from any set of linearly polarized measurements.

Figures 18 through 23 present the results of the statistical analysis of the RCS for six aspect angle regions. An explanation of the double peak on the lower end of the RCS for Figures 18 through 23 is in order. They are caused by all runs being made with one of two gain settings. One corresponds to limiting the minimum measured RCS to approximately -24.8 dBm^2, and the other corresponds to limiting the minimum value to approximately -19.8 dBm^2. Since many values of RCS would normally have been below these levels, the limiting caused peaks in the probability density curves at the limiting levels, and biased the average RCS slightly high. Figure 23 has similar double peaks at the high end of the RCS values. This is due to limiting at the high end.

Some of the raggedness of the curves of the probability density functions for the measured data is probably caused by quantization effects. The measured data are quantized to 0.1 dBm^2 levels. The probability density functions and the cumulative probability functions are computed using 100 intervals, from 0 to 3 σ of the RCS in m^2, and within ± 4 σ of the average for the RCS in dBm^2.

Table 2 contains the tabulated listings of the averages and standard deviations of the RCS in both m^2 and dBm^2. For the sets of data within 30° of nose-on, the average of the vertically polarized RCS is approximately 2 to 3 dB higher than averages of the two circularly polarized RCS which are nearly equal. It is interesting to note that the cross-circularly polarized RCS is higher than the principal circularly polarized RCS for these aspects. The set of data for aspect angles within 15° of broadside is typical of basically specular scattering from convex surfaces. The vertically and principal circularly polarized RCS are nearly the same, and the cross-circularly polarized RCS is down approximately 11 dB. The aspect angle region from 30 to 60° is a

TABLE 2. STATISTICAL CHARACTERISTICS OF THE RADAR CROSS SECTION FOR SELECTED ASPECT ANGLE REGIONS FOR THREE POLARIZATIONS.

Aspect Region	Pol	Avg RCS (m^2)	Std Dev RCS (m^2)	Avg RCS (dBm^2)	Std Dev RCS (dBm^2)
±15° from nose-on	VV	0.140	0.373	-15.3	7.04
	RL	0.0512	0.0890	-17.1	5.71
	LL	0.0769	0.165	-16.8	6.45
GT 15° and LT 30° from nose-on	VV	0.0985	0.215	-15.5	6.63
	RL	0.0523	0.0995	-17.0	5.57
	LL	0.0616	0.154	-16.7	5.57
±30° from nose-on	VV	0.119	0.305	-15.4	6.84
	RL	0.0518	0.198	-17.0	5.64
	LL	0.0693	0.160	-16.7	6.02
GT 30° and LT 60° from nose-on	VV	0.423	2.19	-13.1	7.98
	RL	0.528	3.35	-14.2	7.64
	LL	0.0589	0.215	-16.9	5.34
±60° from nose-on	VV	0.271	1.57	-14.2	7.52
	RL	0.290	2.38	-15.6	6.86
	LL	0.641	0.189	-16.8	5.69
±15° from broadside	VV	154	314	13.7	10.1
	RL	185	381	13.8	10.5
	LL	15.7	40.3	2.83	10.7

transition region. The scattering is due largely to speculars from a number of smaller scatterers. The shape of the probability density function for all of the sets of data are probably best matched with the log-normal distribution. A much better fit would be possible if the data had not been truncated.

These results differ from the measurements on the full size drone. The average RCS for the vertically polarized measurement is significantly lower for the near nose-on aspects.[3] In addition, the probability density functions for the full size drone in the near nose-on aspects was between log-normal and Swerling I for values less than the median. For the near broadside aspect region, the model data are significantly higher than for the full size drone.[4] Both have log-normal probability density functions.

It should be noted that these comparisons are made on sets of measurements which are not the same. The significance of this is hard to evaluate; however, Figures 3 through 6 show clearly that there are obvious differences in measurements made on the two targets.

5. Conclusions and Recommendations

The RCS measurements made on the 0.55 scale model of the MQM-34D at GD/CAD are significantly different from those made at RATSCAT on the full size target. It is believed that the main reason is due to the differences in the targets measured rather than differences in the ranges. This means that considerable care must be used in evaluating system performance using the DSM of the radar signature.

The differences between the principal and cross-circular polarization RCS are negligible for aspect angles within 30° of nose-on, and each is only 2 to 3 dB lower than the vertical polarization RCS. This indicates that a radar system using cross-circular polarization for

---

[3] Wright, J. W., On the Statistical Analysis of the Radar Signature of the MQM-34D, Interim Report Number 1, Technical Report RE-75-7, US Army Missile Command, Redstone Arsenal, Alabama, 2 October 1974.

[4] Wright, J. W., On the Statistical Analysis of the Radar Signature of the MQM-34D, Interim Report Number 2, Technical Report RE-75-13, US Army Missile Command, Redstone Arsenal, Alabama, 31 January 1975.

improved performance in rain would pay only a negligible penalty in performance. This result should be investigated further to verify the conclusion for other types of targets.

An investigation should be made into the requirements for construction of models for radar signature measurements. It is apparent that the models should not have continuous conductive skins. However, just breaking the conductivity at natural joints may cause even more problems by introducing EM structures which are no more representative of the actual target than the continuous conductive skin model. The problem of modeling techniques and accuracy from the overall EM viewpoint does not appear to have had (nor presently have) adequate importance or financial support. However, if model measurements are to be meaningful, the problem of model building must be resolved.

A summary of statistical characteristics of the radar signature of the MQM-34D near normal to the roll axis (vertical polarization) is given in Table 3.

TABLE 3. SUMMARY OF STATISTICAL CHARACTERISTICS OF THE RADAR SIGNATURE OF THE MQM-34D NEAR NORMAL TO THE ROLL AXIS (VERTICAL POLARIZATION)

Parameter	Bistatic Angle (deg)			
	0	10	20	30
	Within 15° of normal to roll axis			
Average of RCS (m^2)	42.550	41.816	46.116	45.130
Std Dev of RCS (m^2)	130.689	161.282	135.130	129.195
Average of RCS (dBm^2)	8.915	9.181	9.094	9.879
Std Dev of RCS (dBm^2)	8.452	8.266	8.485	8.004
Average of Glint (ft)	-2.617	---	---	-0.0986
Std Dev of Glint (ft)	10.259	---	---	6.205
	Within 30° of normal to roll axis			
Average of RCS (m^2)	21.352	19.991	28.872	22.395
Std Dev of RCS (m^2)	92.443	72.220	95.857	91.767
Average of RCS (dBm^2)	3.174	2.641	2.559	3.043
Std Dev of RCS (dBm^2)	9.461	9.828	10.059	9.956
Average of Glint (ft)	-1.439	---	---	-0.262
Std Dev of Glint (ft)	10.005	---	---	5.536

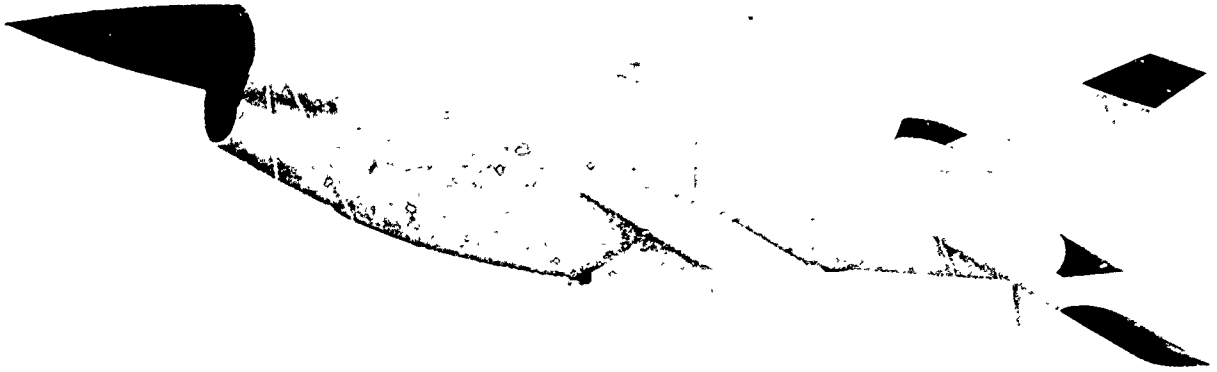

Figure 1. Photograph of model of MQM-34D.

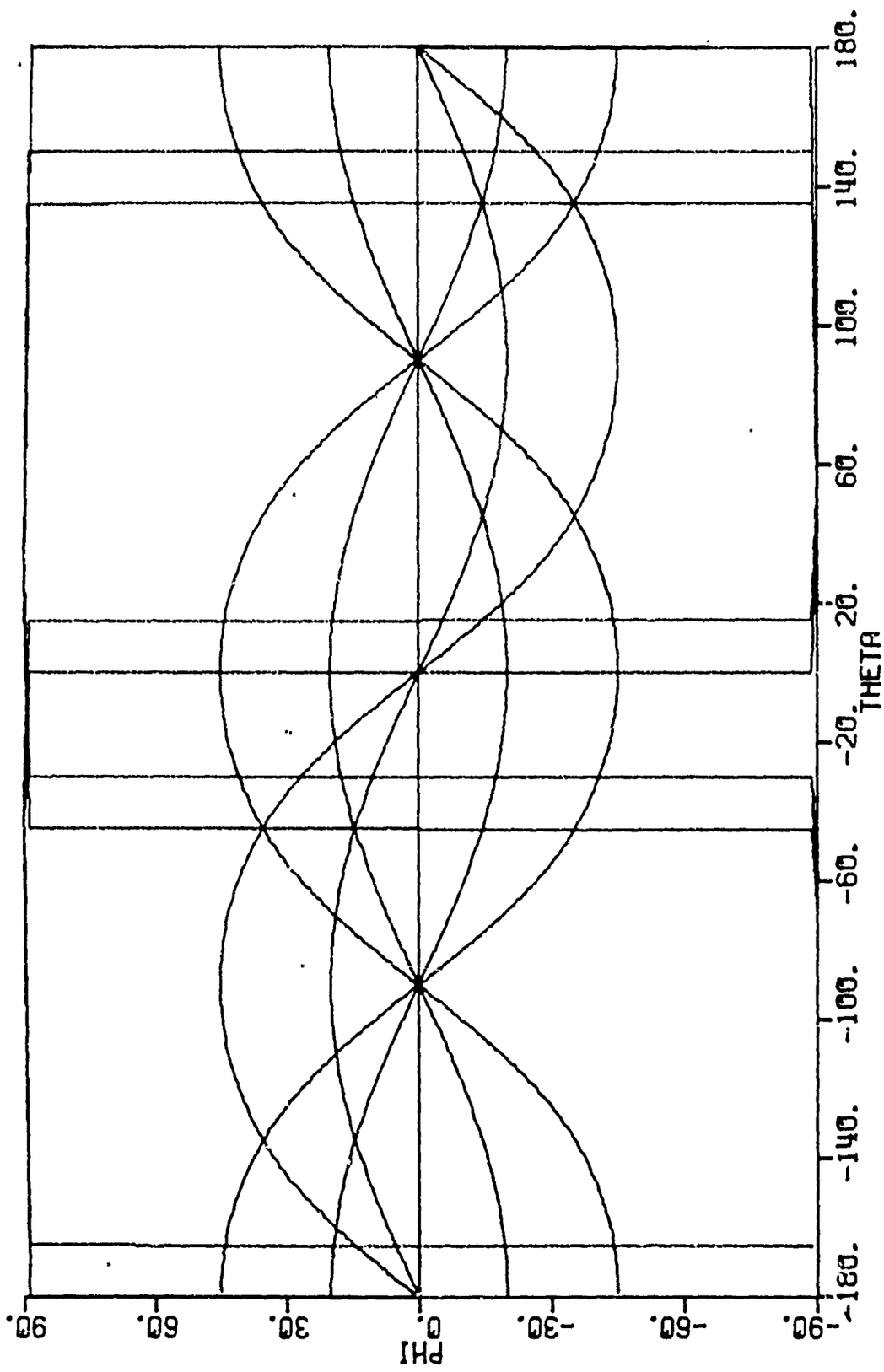

Figure 2. Plots of aspect angles for the data cuts.

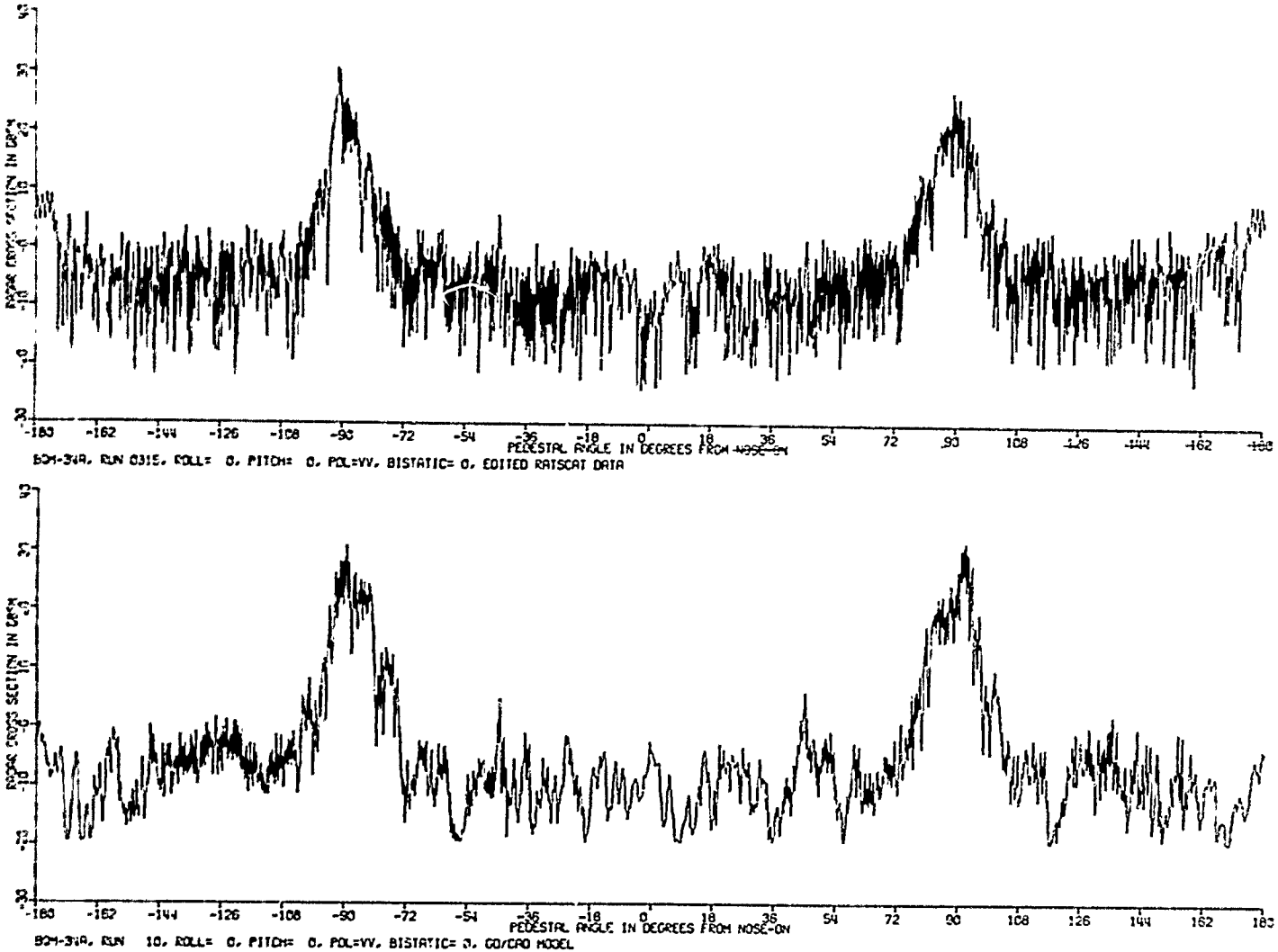

Figure 3. Measured RCS on 0.55 scale model and full size BQM-34A, 0° pitch, 0° roll, vertical polarization.

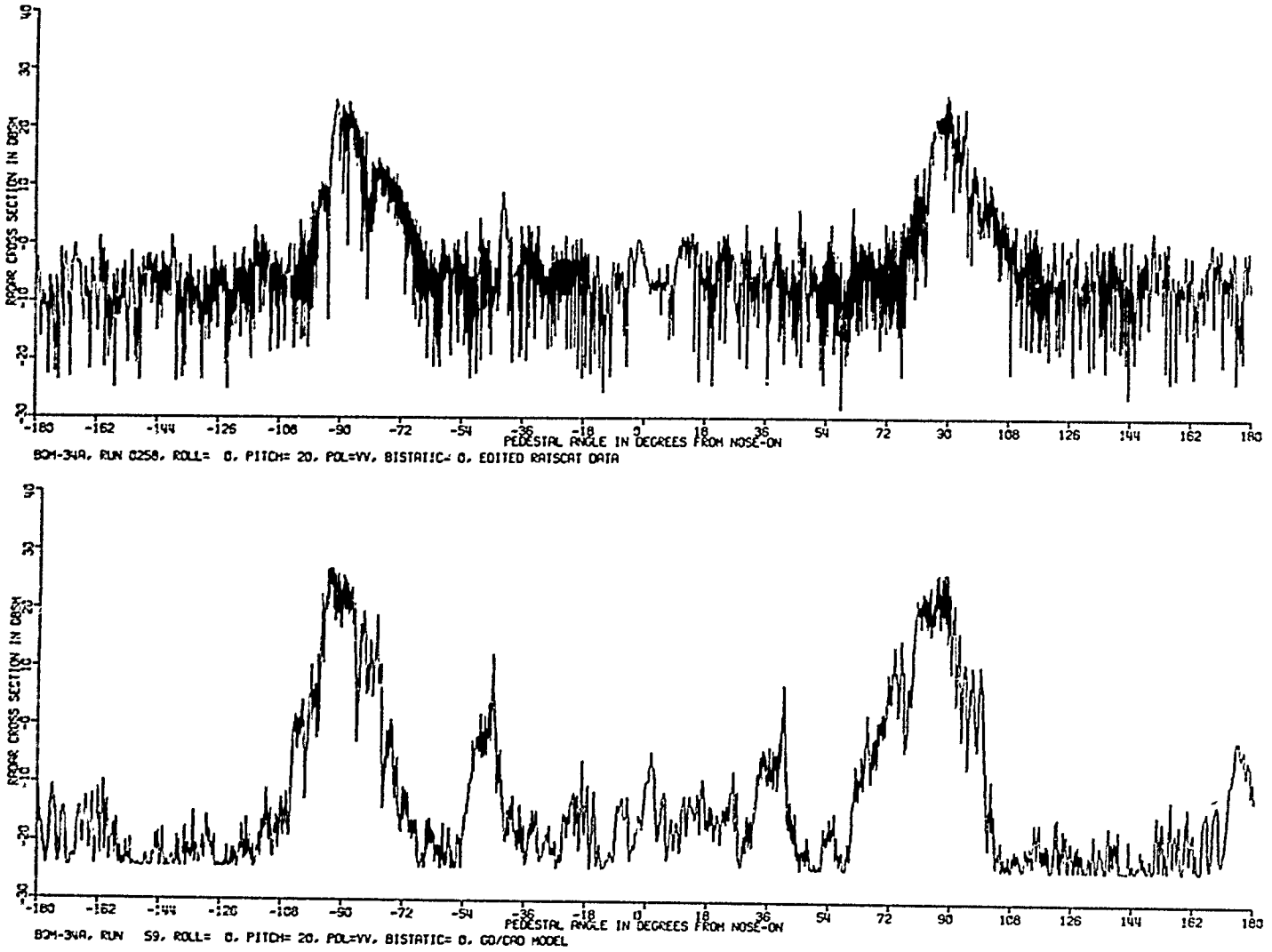

Figure 4. Measured RCS on 0.55 scale model and full size BQM-34A, 20° pitch, 0° roll, vertical polarization.

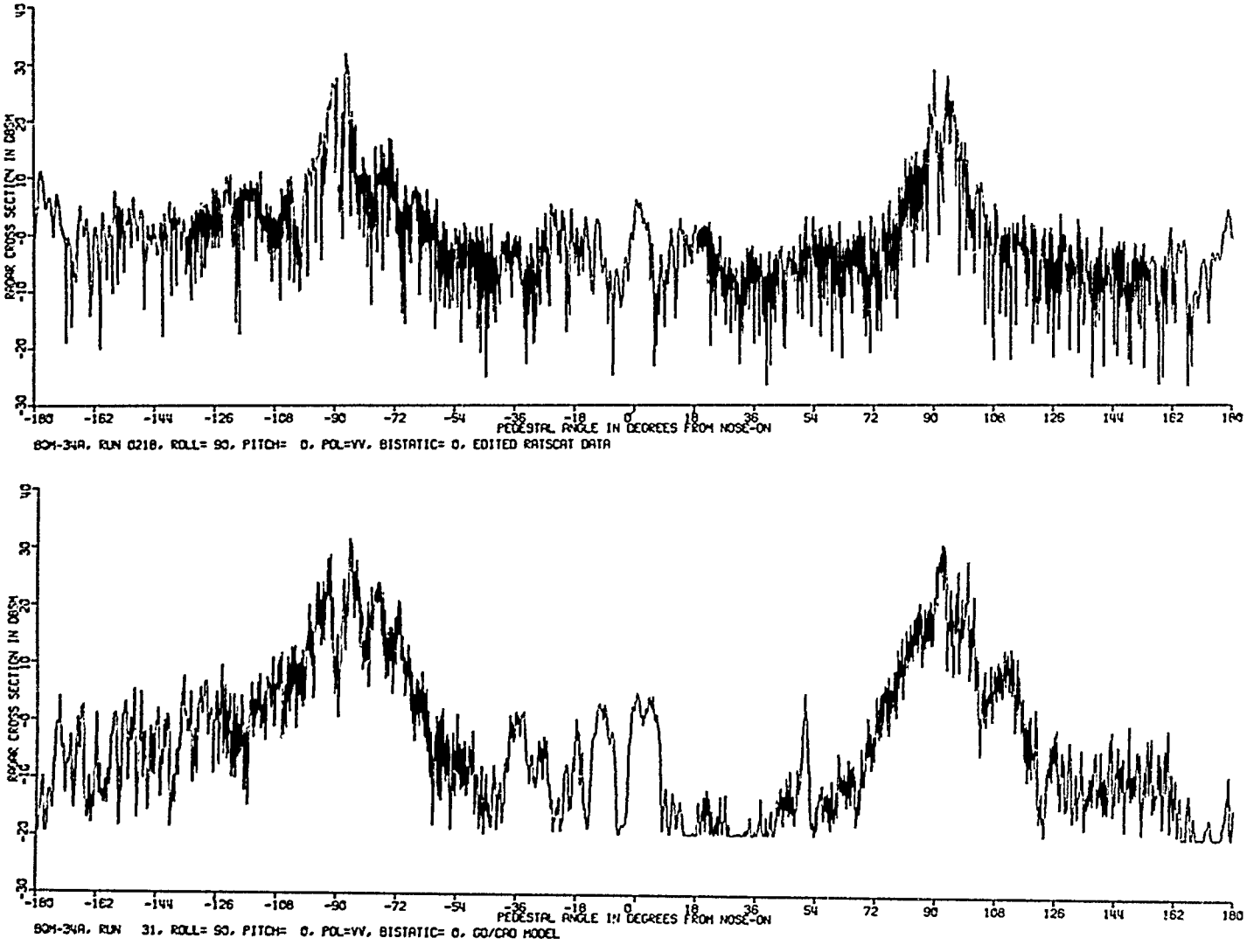

Figure 5. Measured RCS on 0.55 scale model and full size BQM-34A, 0° pitch, 20° roll, vertical polarization.

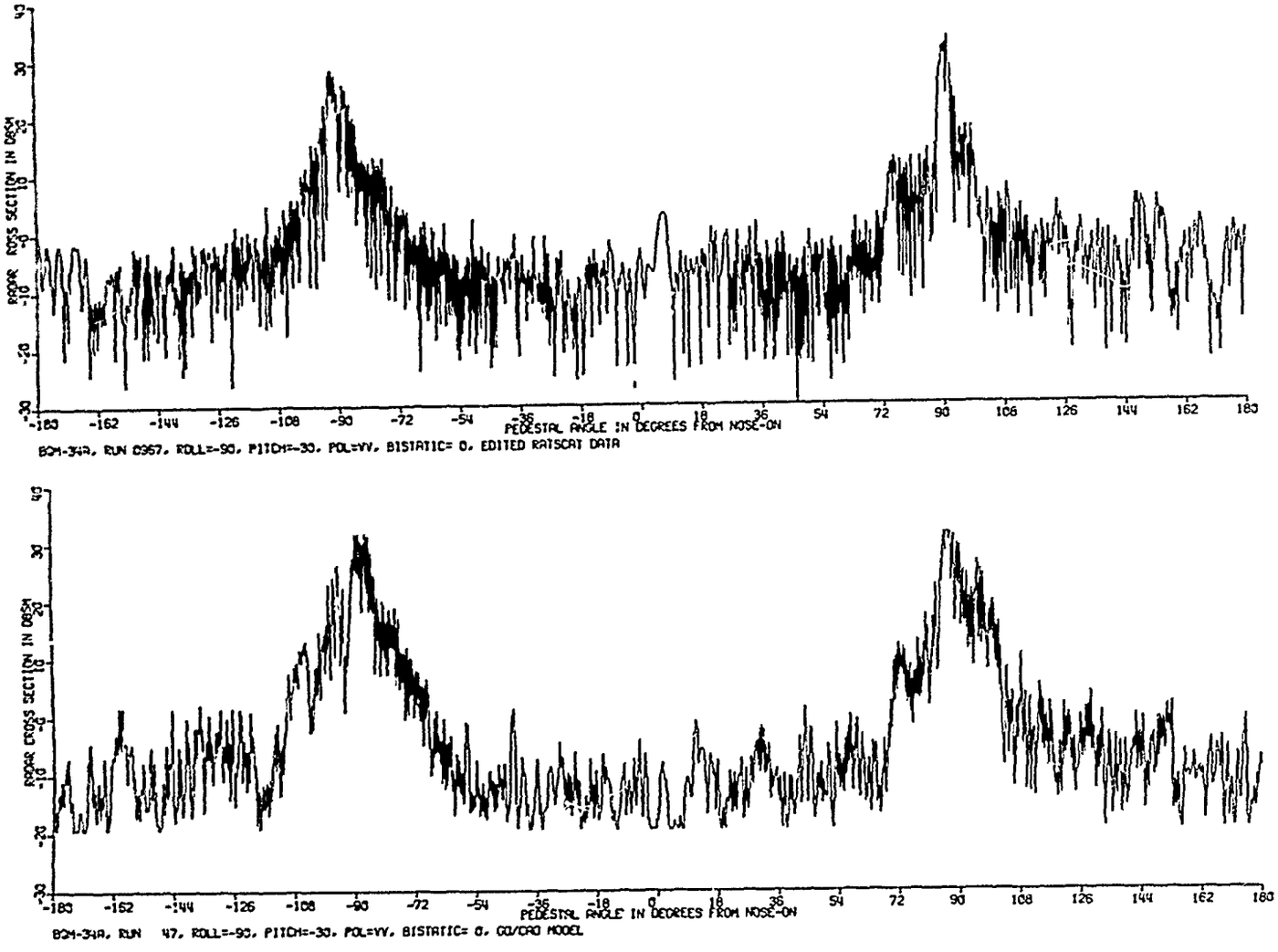

Figure 6. Measured RCS on 0.55 scale model and full size BQM-34A, -30° pitch, -90° roll, vertical polarization.

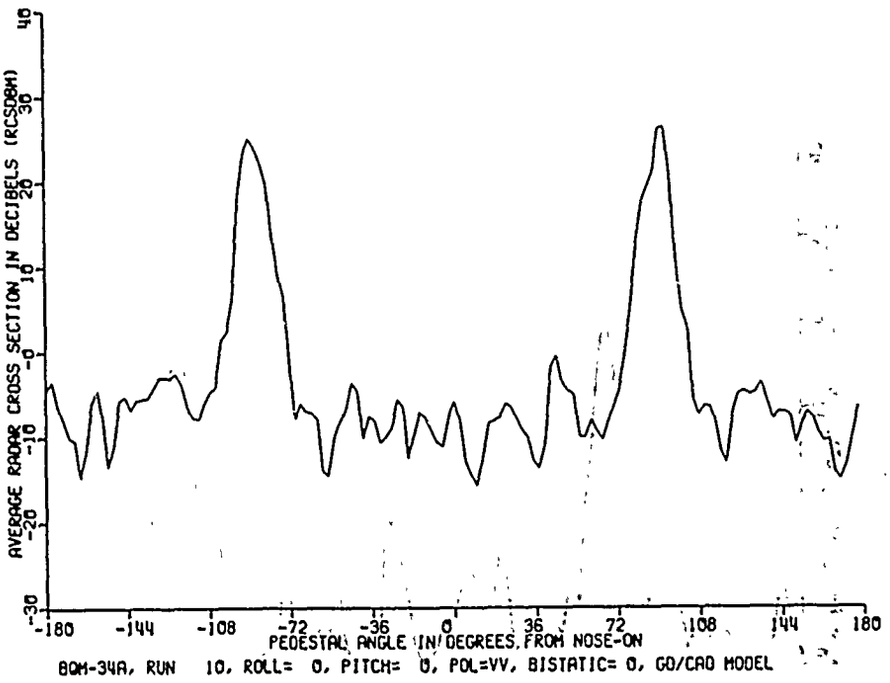

BQM-34A, RUN 10, ROLL= 0, PITCH= 0, POL=VV, BISTATIC= 0, GO/CAO MODEL

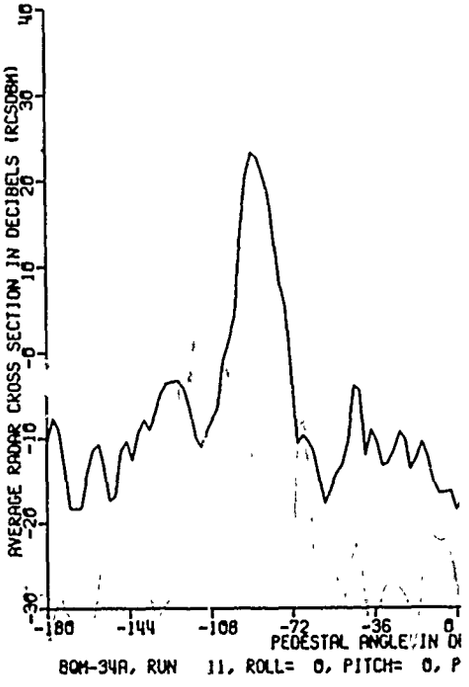

BQM-34A, RUN 11, ROLL= 0, PITCH= 0, P

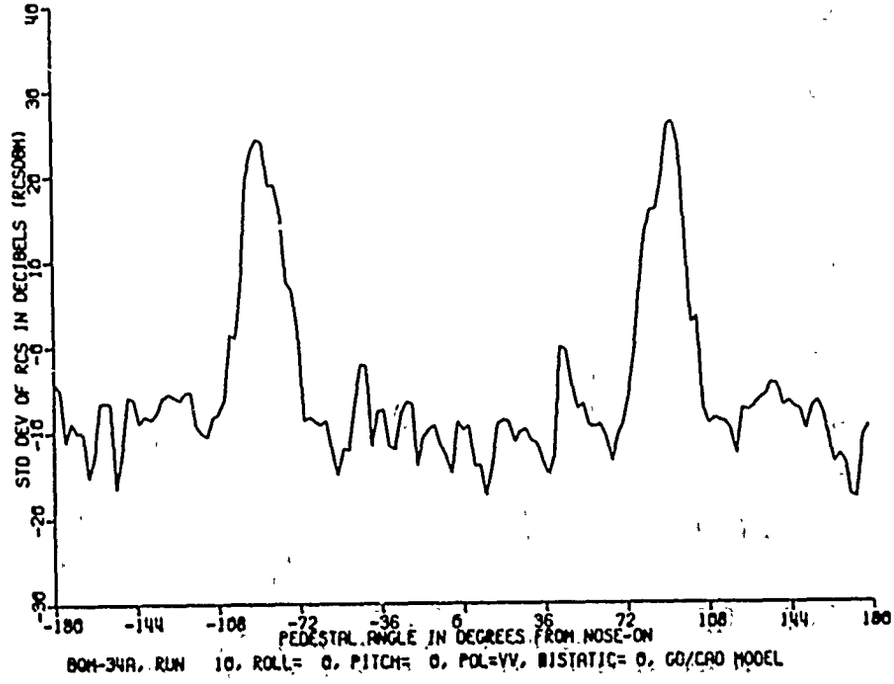

BQM-34A, RUN 10, ROLL= 0, PITCH= 0, POL=VV, BISTATIC= 0, GO/CAO MODEL

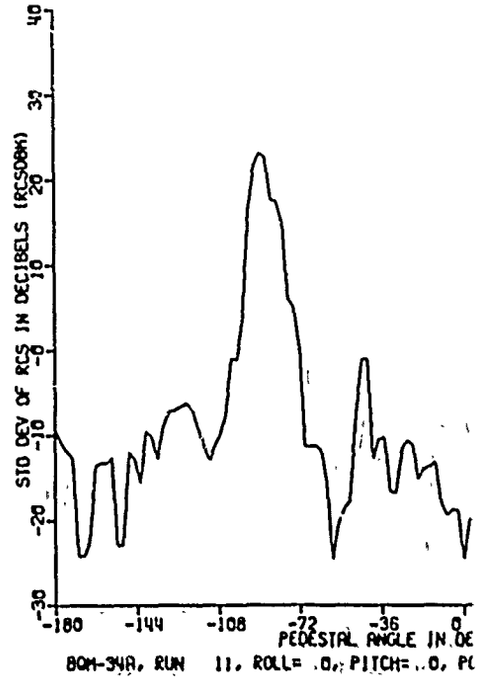

BQM-34A, RUN 11, ROLL= 0, PITCH= 0, P

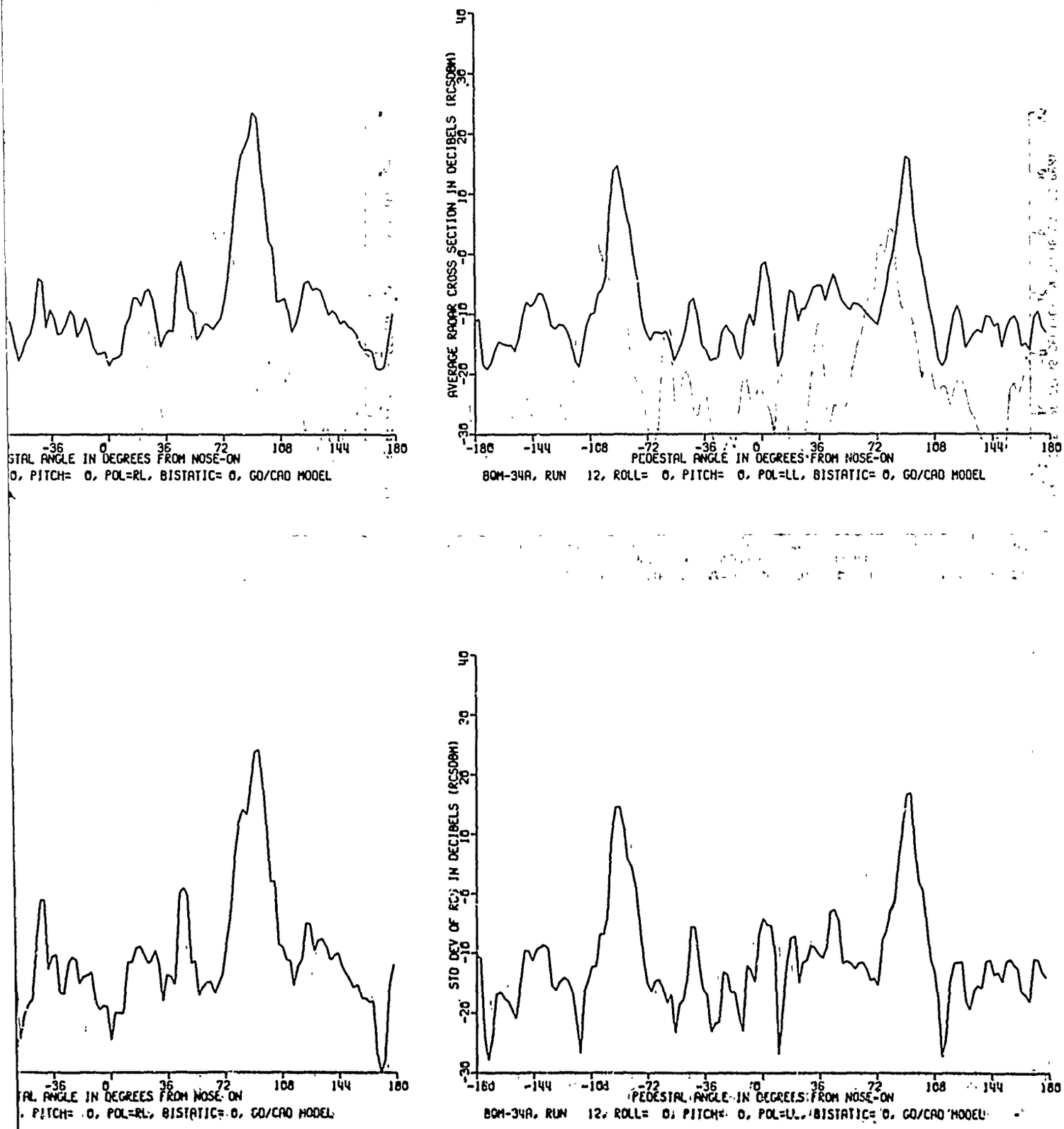

Figure 7. Average and standard deviation of measured RCS, 0° pitch, 0° roll.

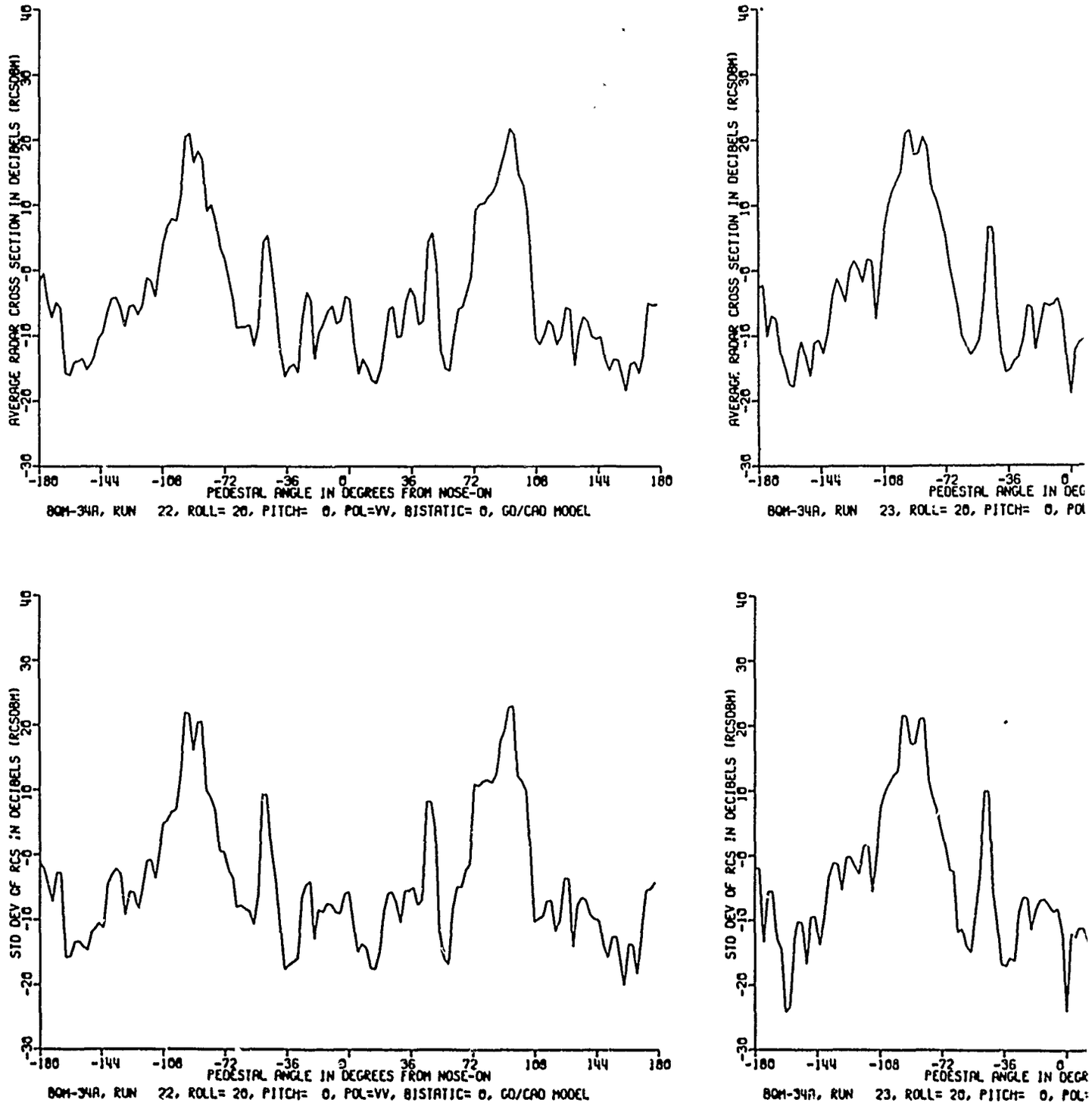

Figure 8. Average and standard deviation of measured RCS, 0° pitch, 20° roll.

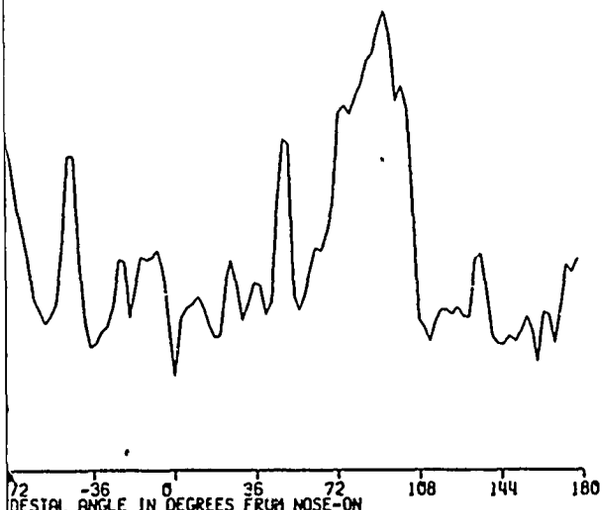

20, PITCH= 0, POL=RL, BISTATIC= 0, GO/CAD MODEL

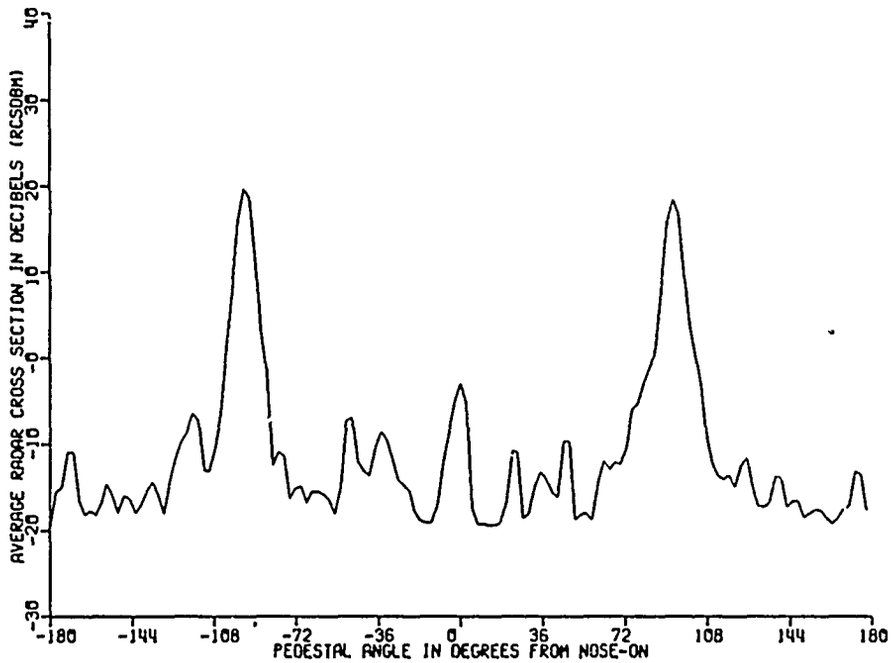

8QM-34A, RUN 24, ROLL= 20, PITCH= 0, POL=LL, BISTATIC= 0, GO/CAD MODEL

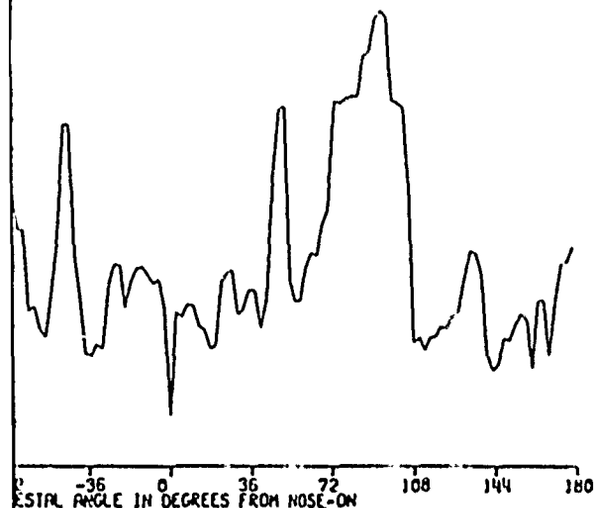

20, PITCH= 0, POL=RL, BISTATIC= 0, GO/CAD MODEL

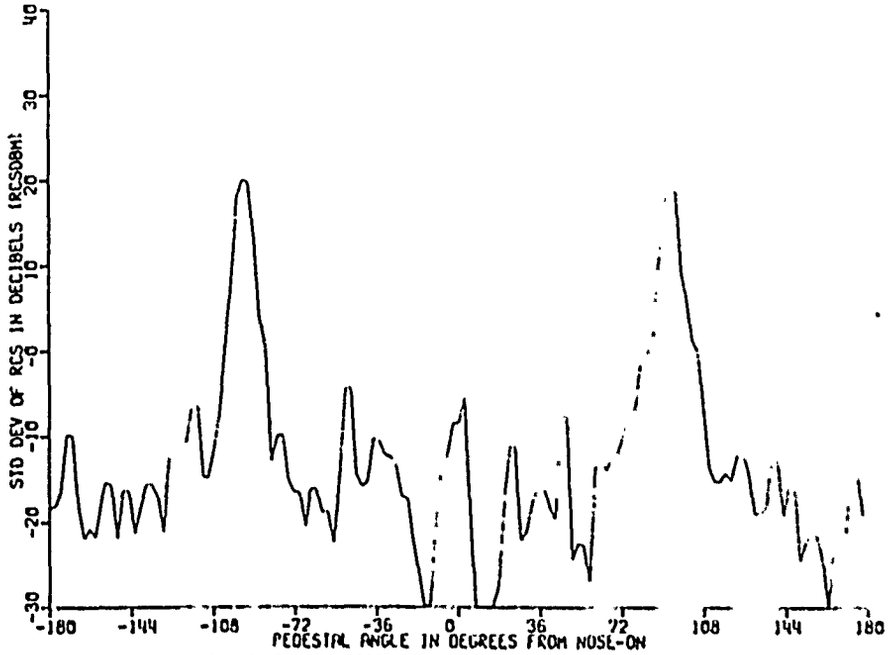

8QM-34A, RUN 24, ROLL= 20, PITCH= 0, POL=LL, BISTATIC= 0, GO/CAD MODEL

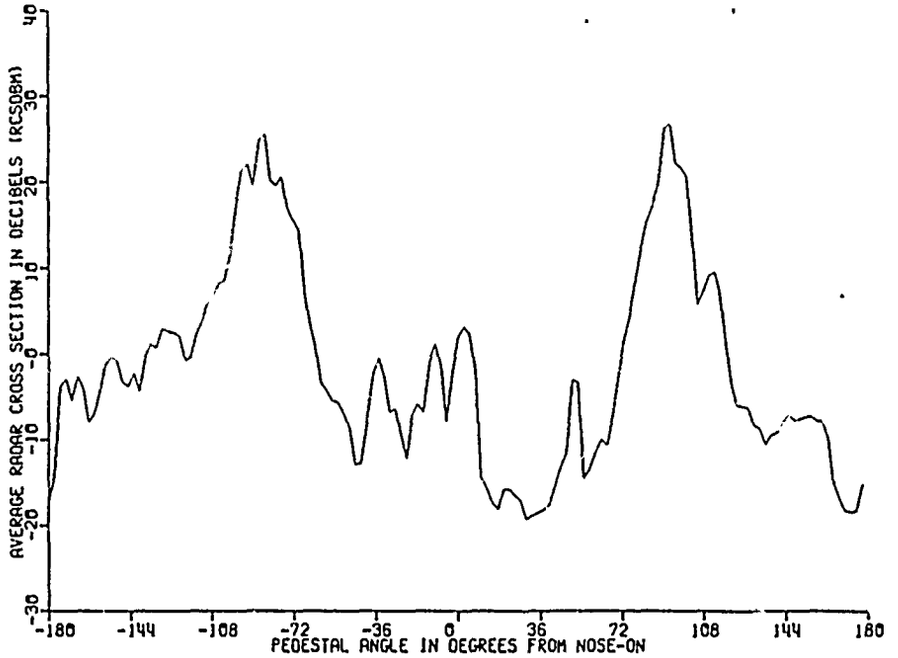

BQM-34A, RUN 31, ROLL= 90, PITCH= 0, POL=VV, BISTATIC= 0, GO/CAD MODEL

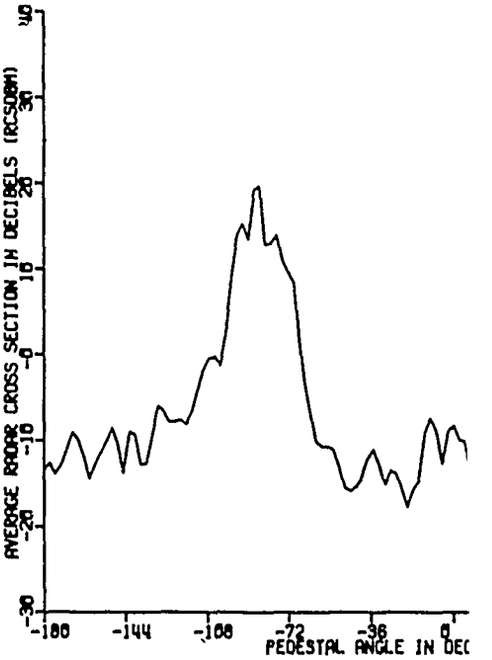

BQM-34A, RUN 32, ROLL= 90, PITCH= 0, POL

BQM-34A, RUN 31, ROLL= 90, PITCH= 0, POL=VV, BISTATIC= 0, GO/CAD MODEL

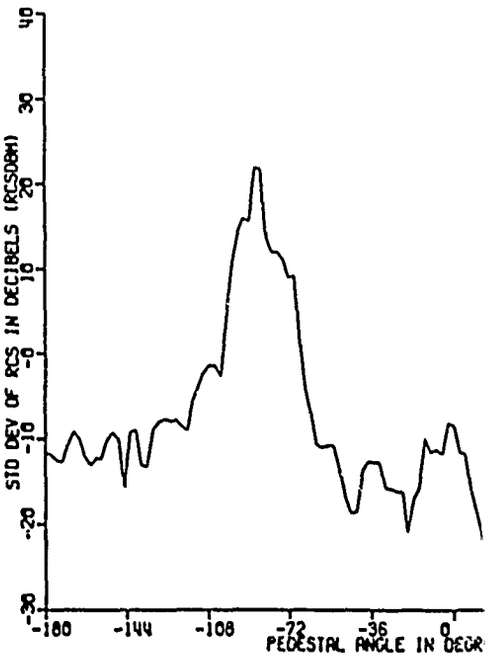

BQM-34A, RUN 32, ROLL= 90, PITCH= 0, POL=

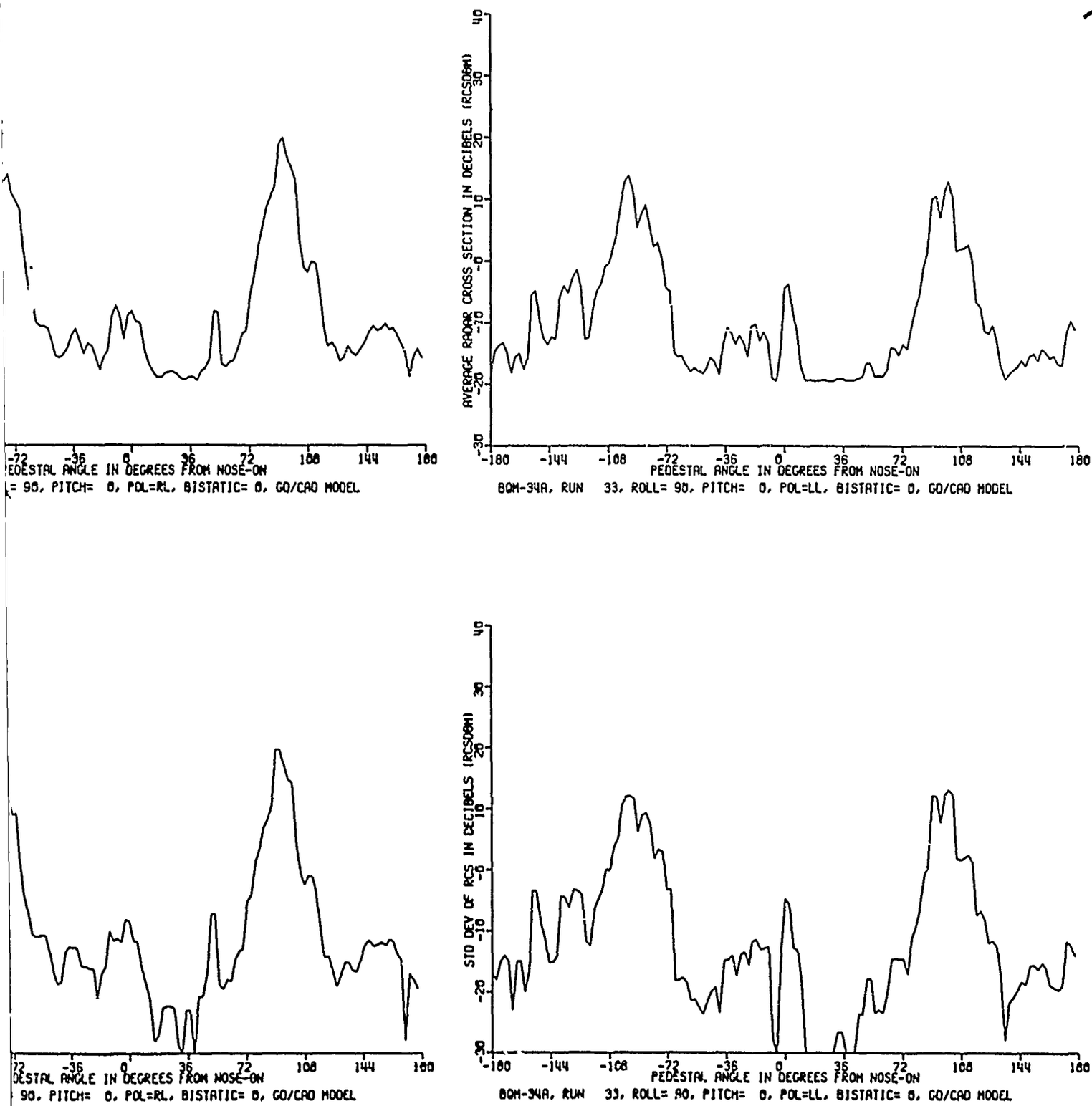

Figure 9. Average and standard deviation of measured RCS, 0° pitch, 90° roll.

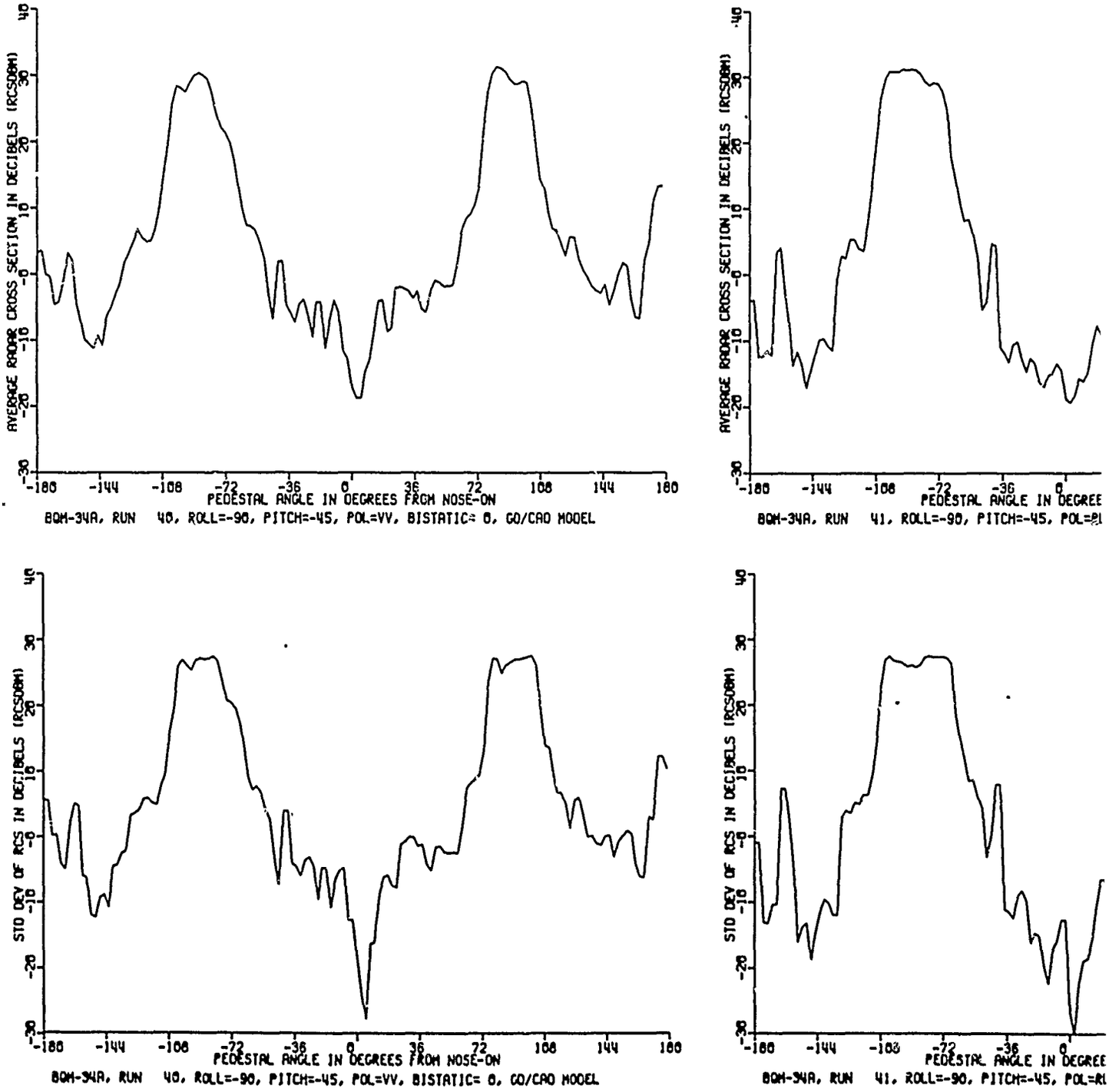

Figure 10. Average and standard deviation of measured RCS, -45° pitch, -90° roll.

1

2

TAL ANGLE IN DEGREES FROM NOSE-ON

, PITCH=-45, POL=RL, BISTATIC= 0, GO/CAD MODEL

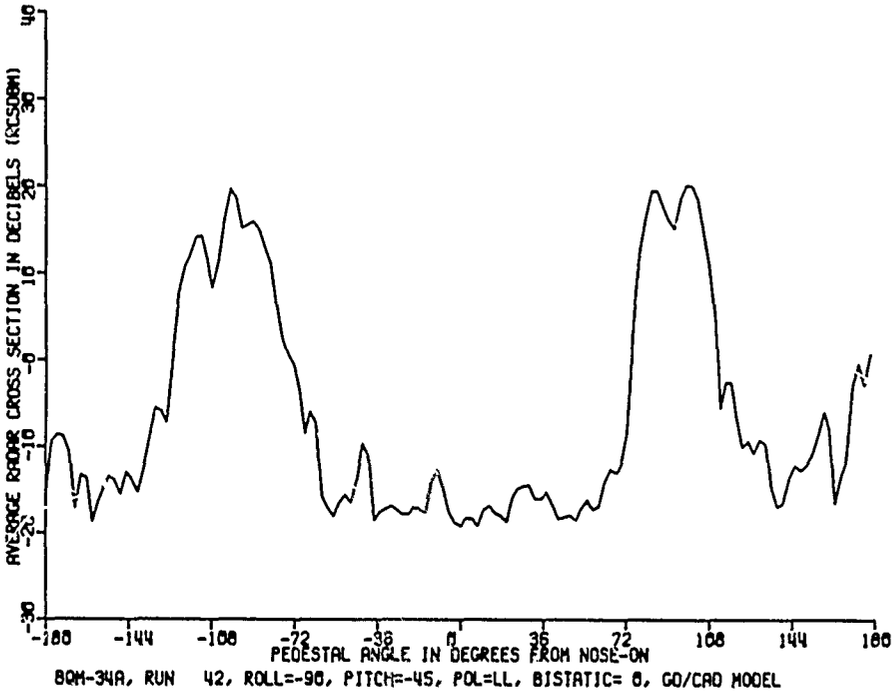

BQM-34A, RUN 42, ROLL=-90, PITCH=-45, POL=LL, BISTATIC= 0, GO/CAD MODEL

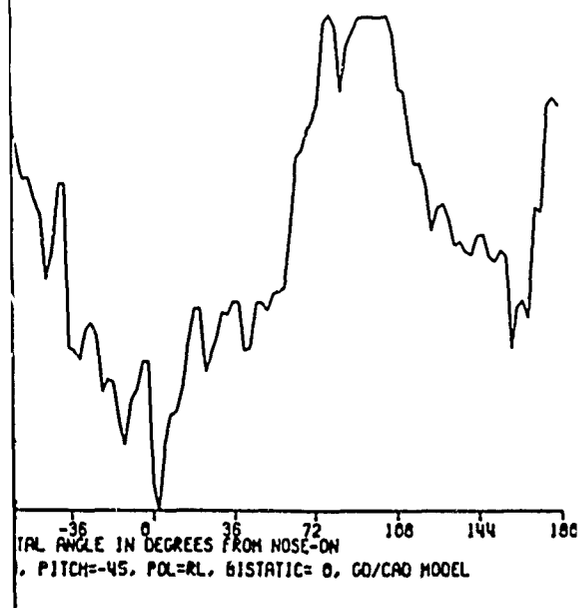

TAL ANGLE IN DEGREES FROM NOSE-ON

, PITCH=-45, POL=RL, BISTATIC= 0, GO/CAD MODEL

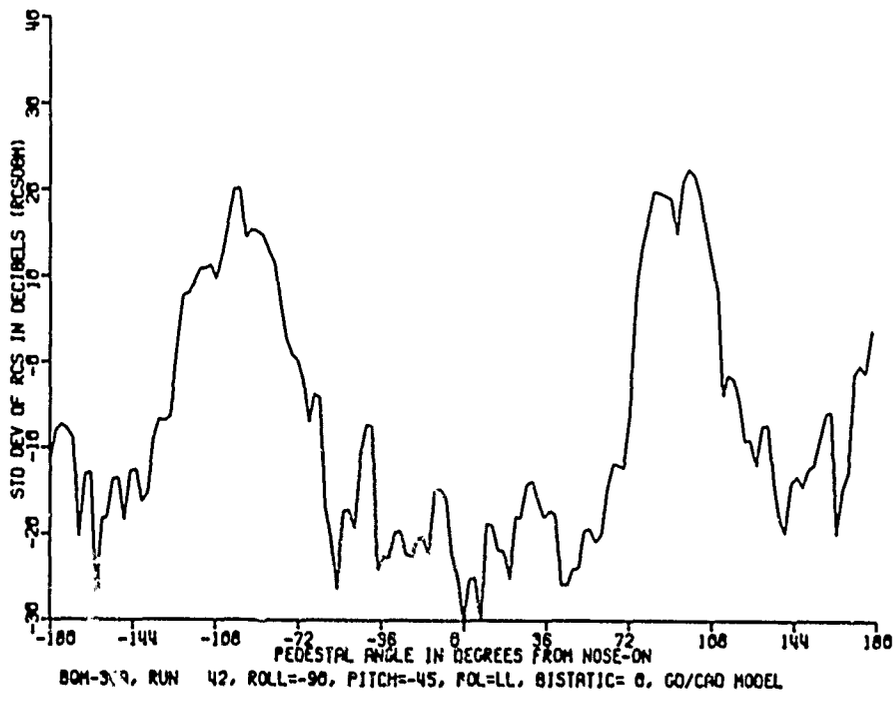

BQM-34A, RUN 42, ROLL=-90, PITCH=-45, POL=LL, BISTATIC= 0, GO/CAD MODEL

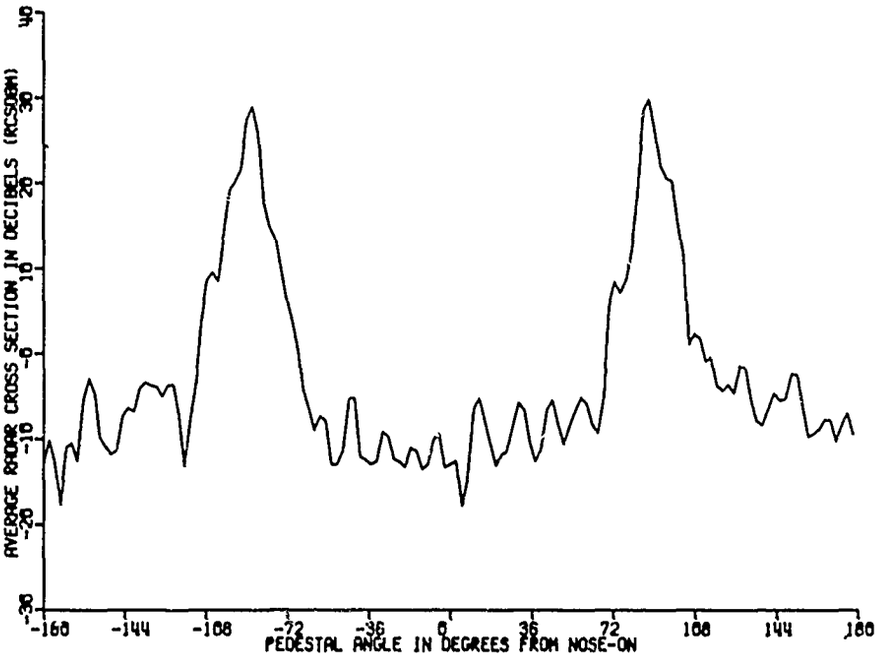

BQM-34A, RUN 47, ROLL=-90, PITCH=-30, POL=VV, BISTATIC= 0, GO/CAD MODEL

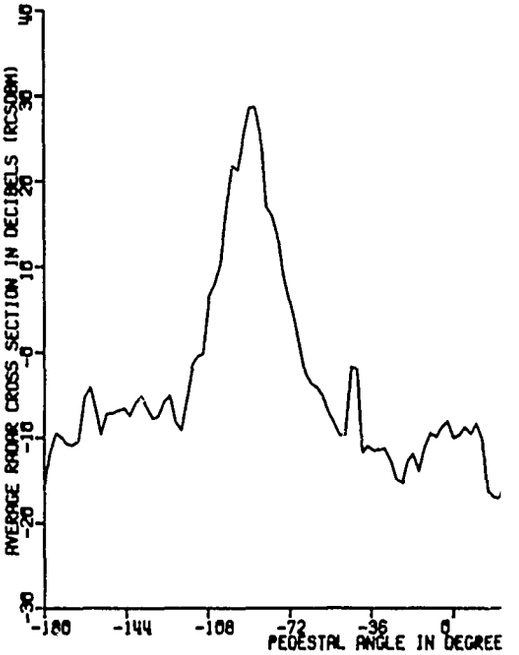

BQM-34A, RUN 48, ROLL=-90, PITCH=-30, POL=R

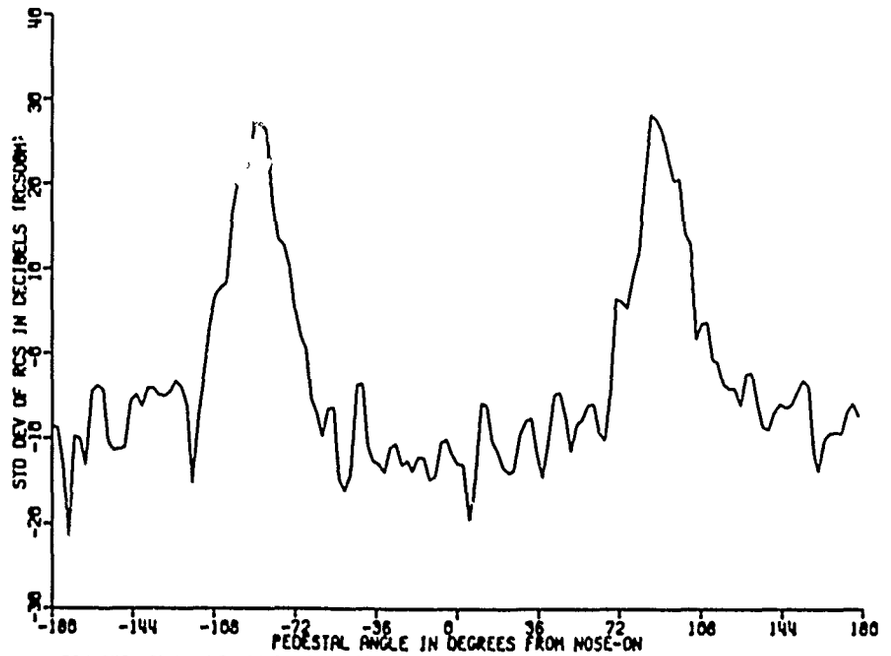

BQM-34A, RUN 47, ROLL=-90, PITCH=-30, POL=VV, BISTATIC= 0, GO/CAD MODEL

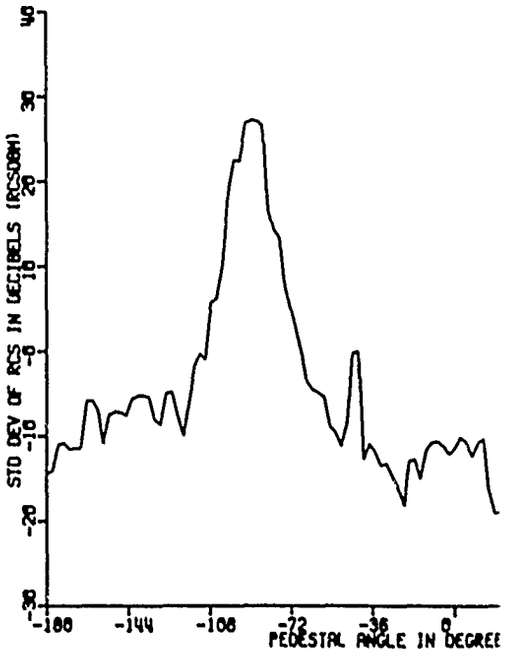

BQM-34A, RUN 48, ROLL=-90, PITCH=-30, POL=R

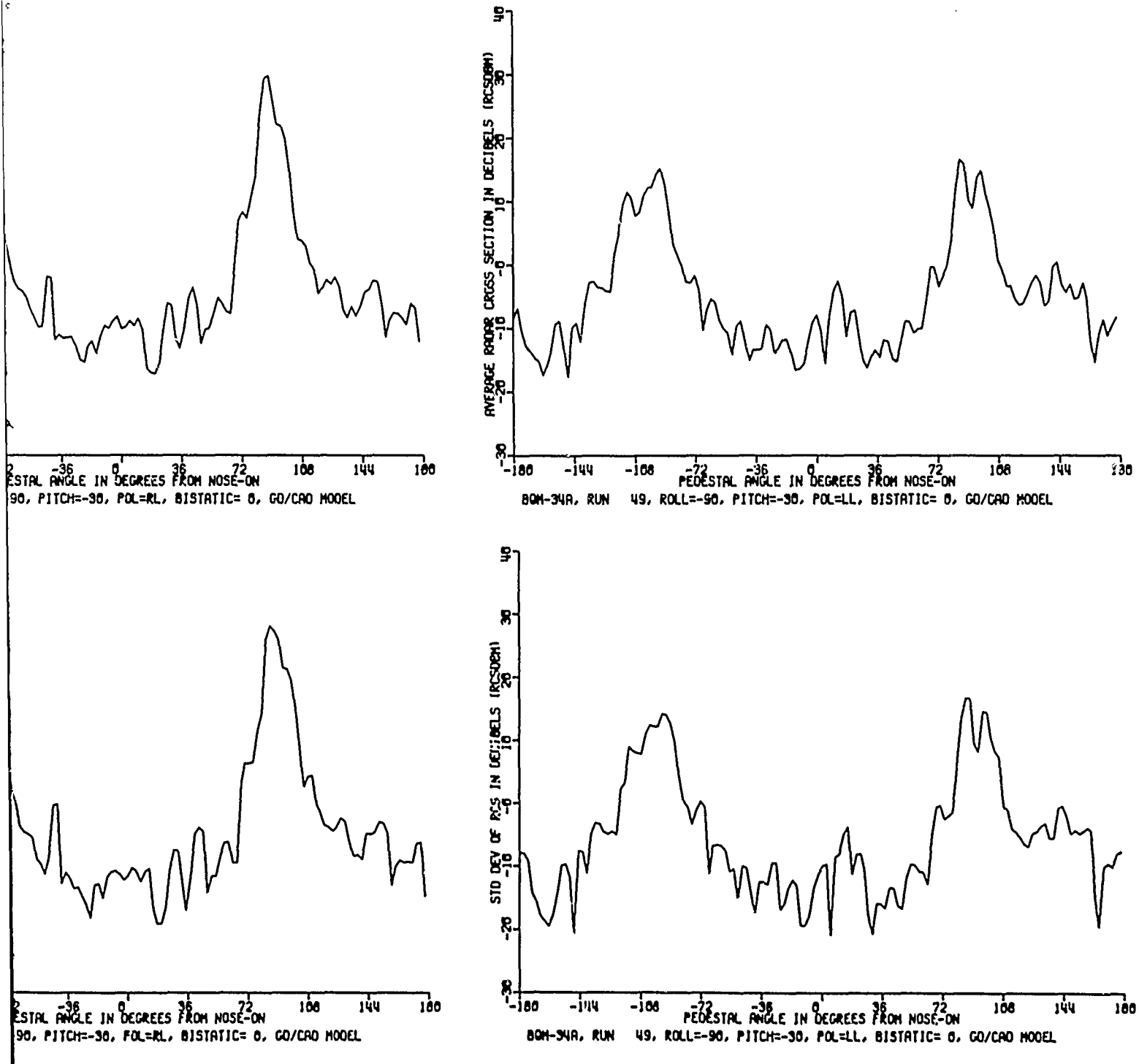

Figure 11. Average and standard deviation of measured RCS, -30° pitch, -90° roll.

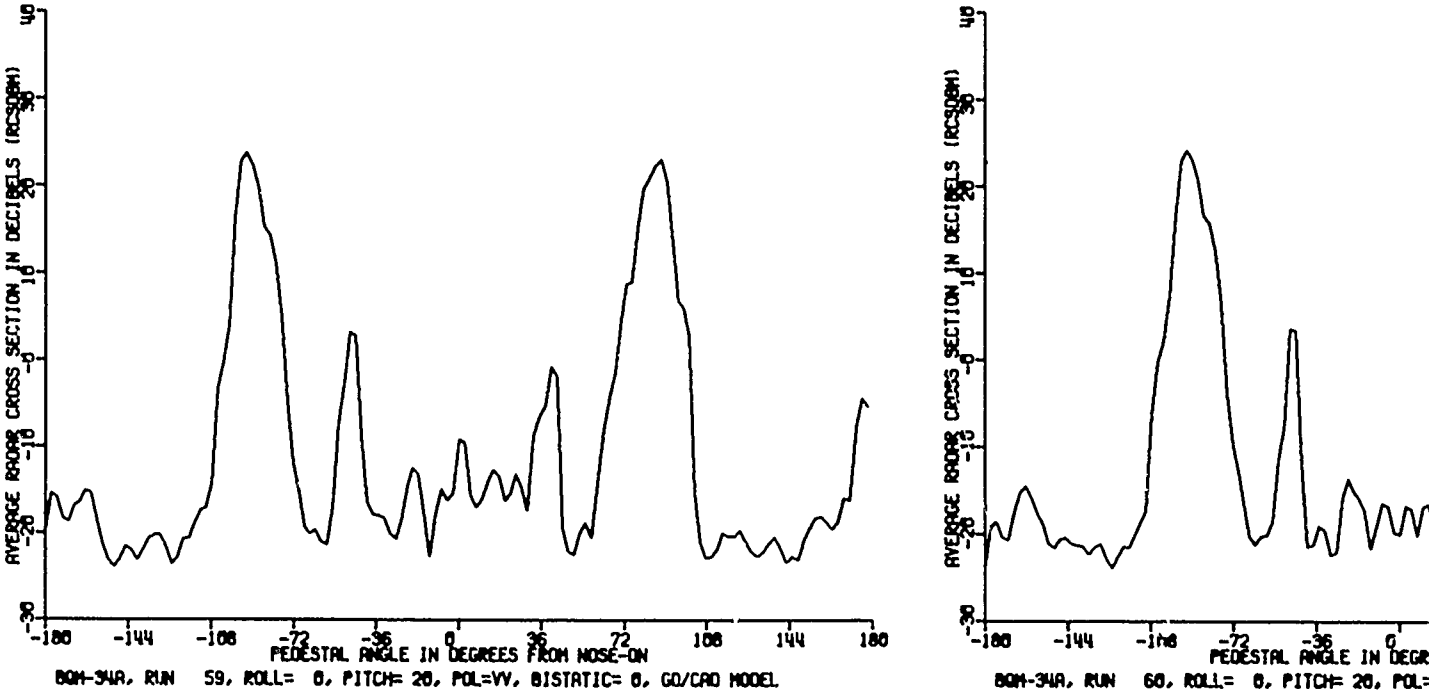

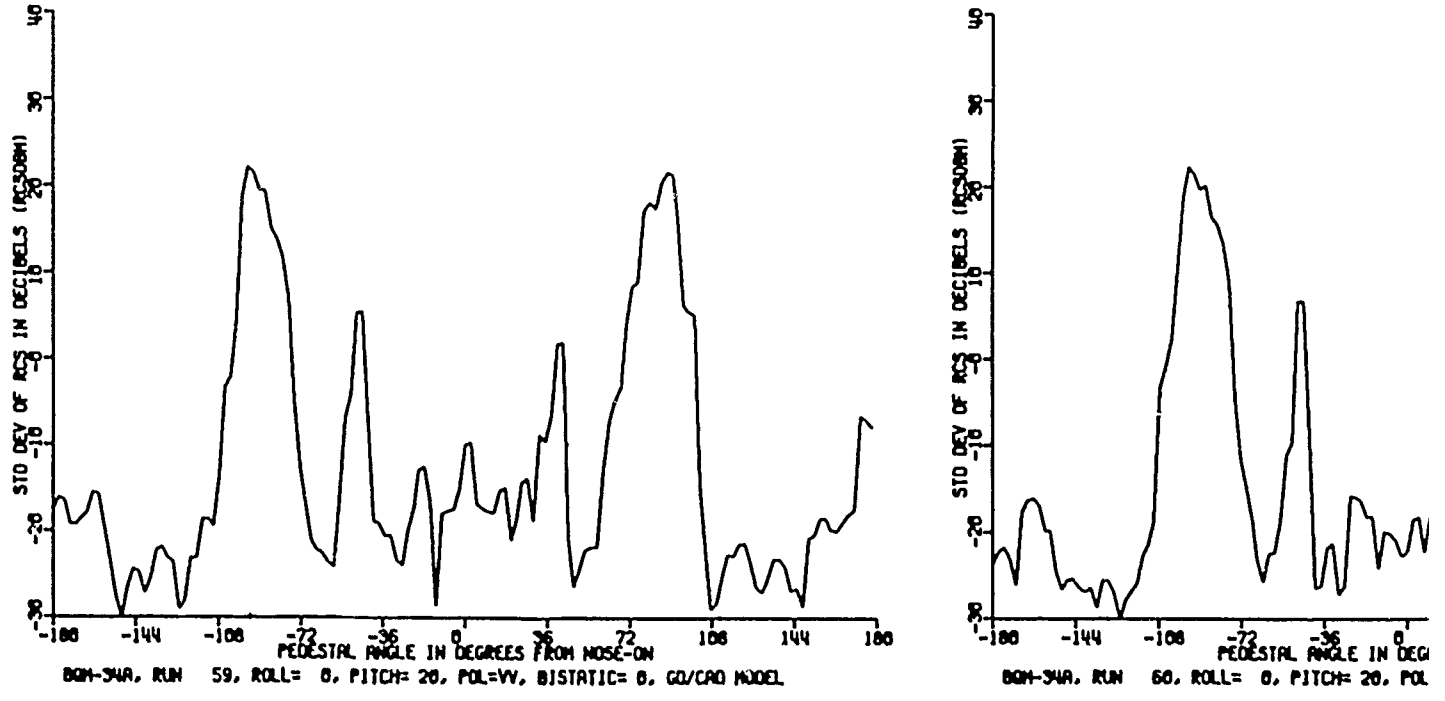

Figure 12. Average and standard deviation of measured RCS, 20° pitch, 0° roll.

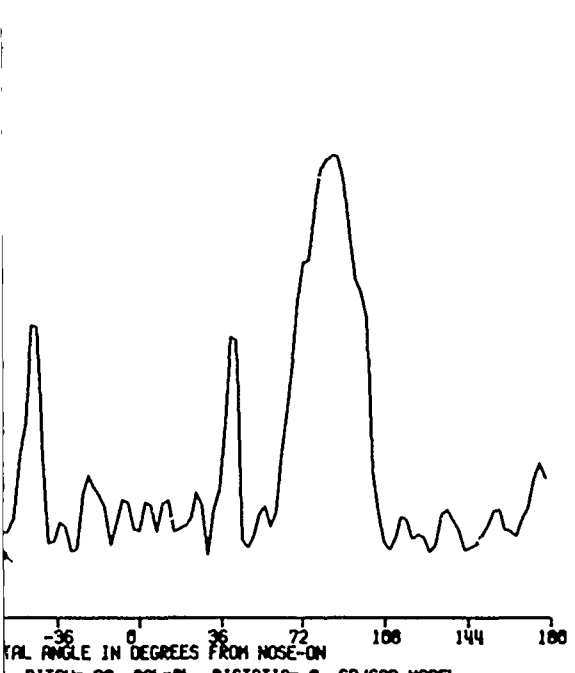

TAL ANGLE IN DEGREES FROM NOSE-ON
, PITCH= 20, POL=RL, BISTATIC= 0, GD/CAD MODEL

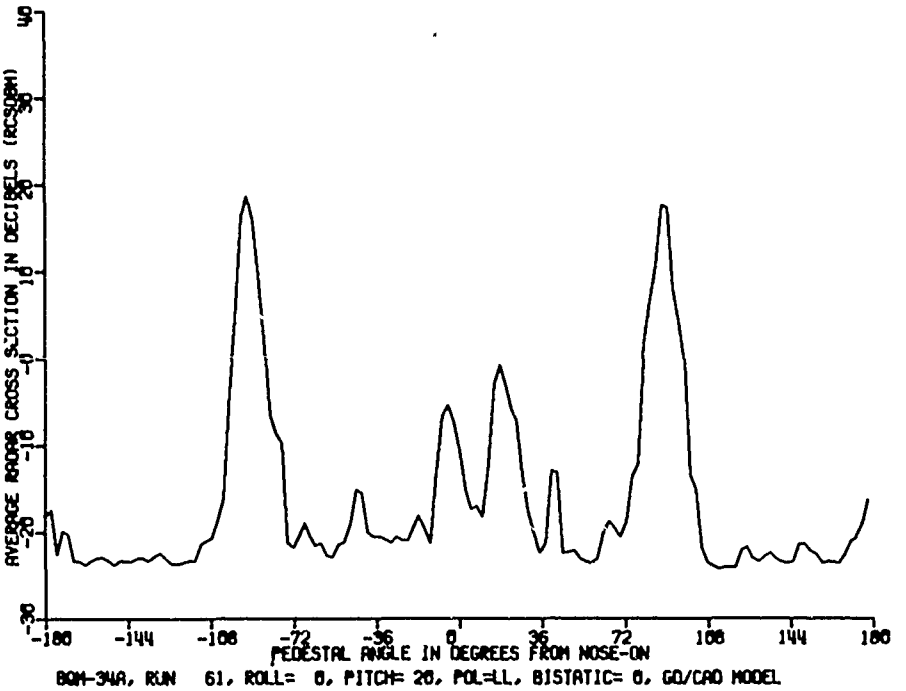

BQM-34A, RUN 61, ROLL= 0, PITCH= 20, POL=LL, BISTATIC= 0, GD/CAD MODEL

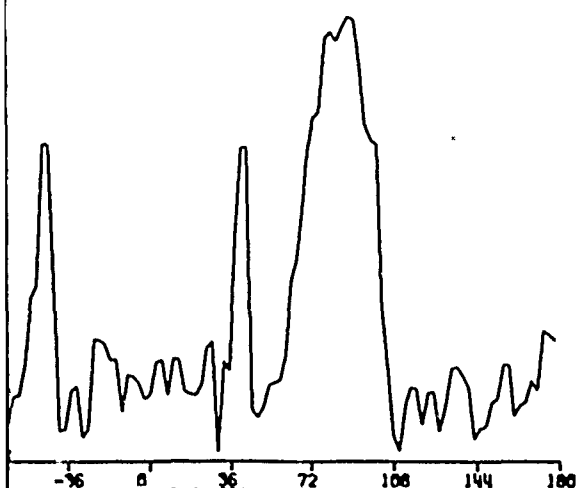

TAL ANGLE IN DEGREES FROM NOSE-ON
0, PITCH= 20, POL=RL, BISTATIC= 0, GD/CAD MODEL

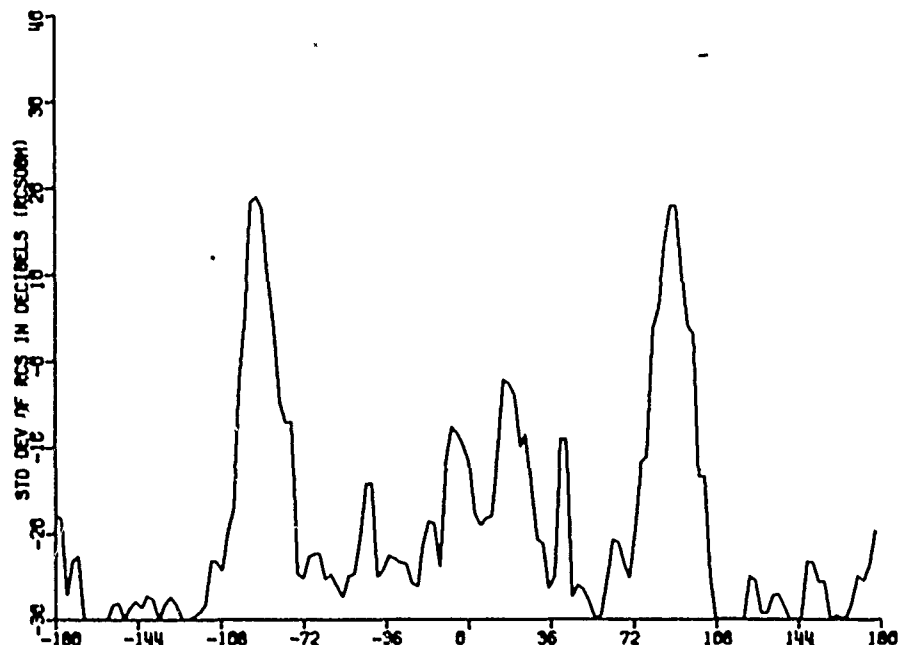

BQM-34A, RUN 61, ROLL= 0, PITCH= 20, POL=LL, BISTATIC= 0, GD/CAD MODEL

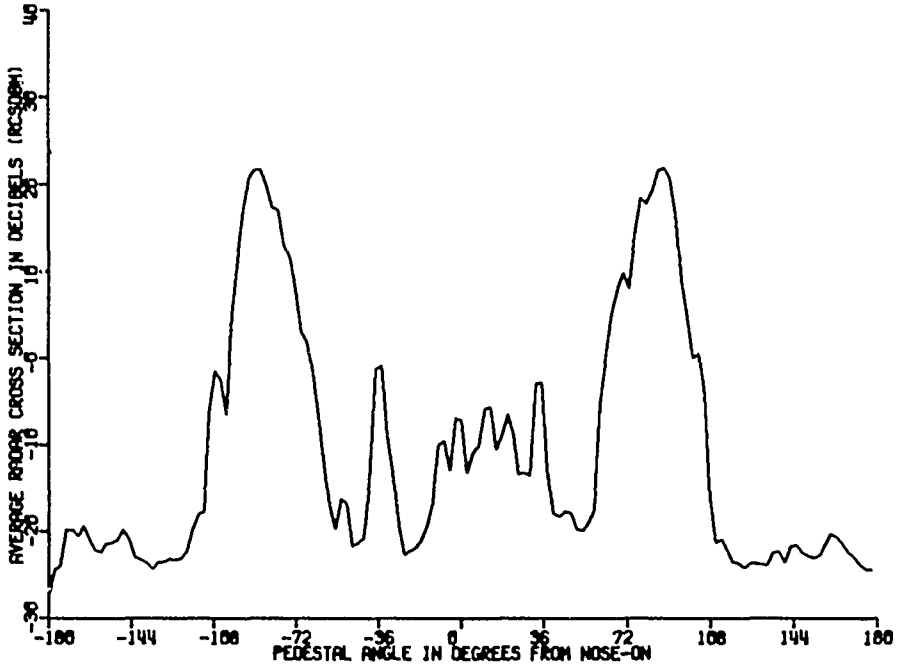

BOM-34A, RUN 64, ROLL= 0, PITCH= 45, POL=VV, BISTATIC= 0, GO/CAD MODEL

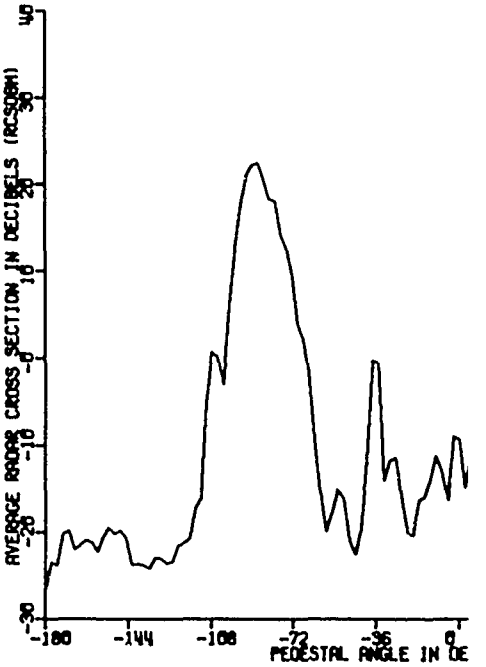

BOM-34A, RUN 63, ROLL= 0, PITCH= 45, PO

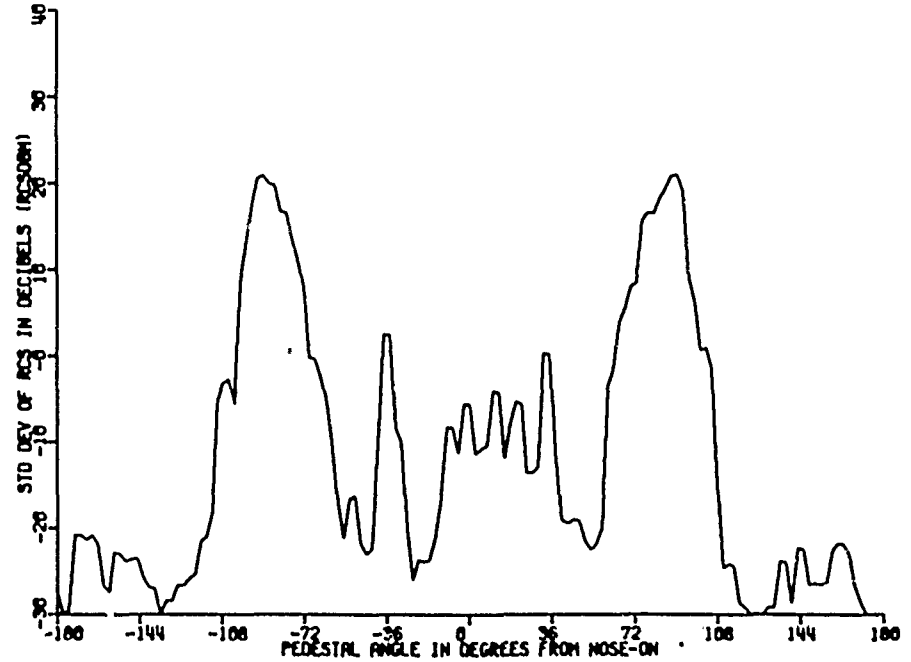

BOM-34A, RUN 64, ROLL= 0, PITCH= 45, POL=VV, BISTATIC= 0, GO/CAD MODEL

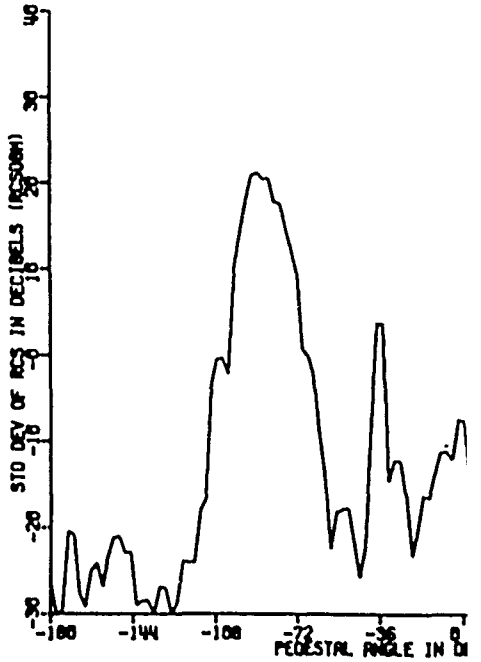

BOM-34A, RUN 63, ROLL= 0, PITCH= 45, P

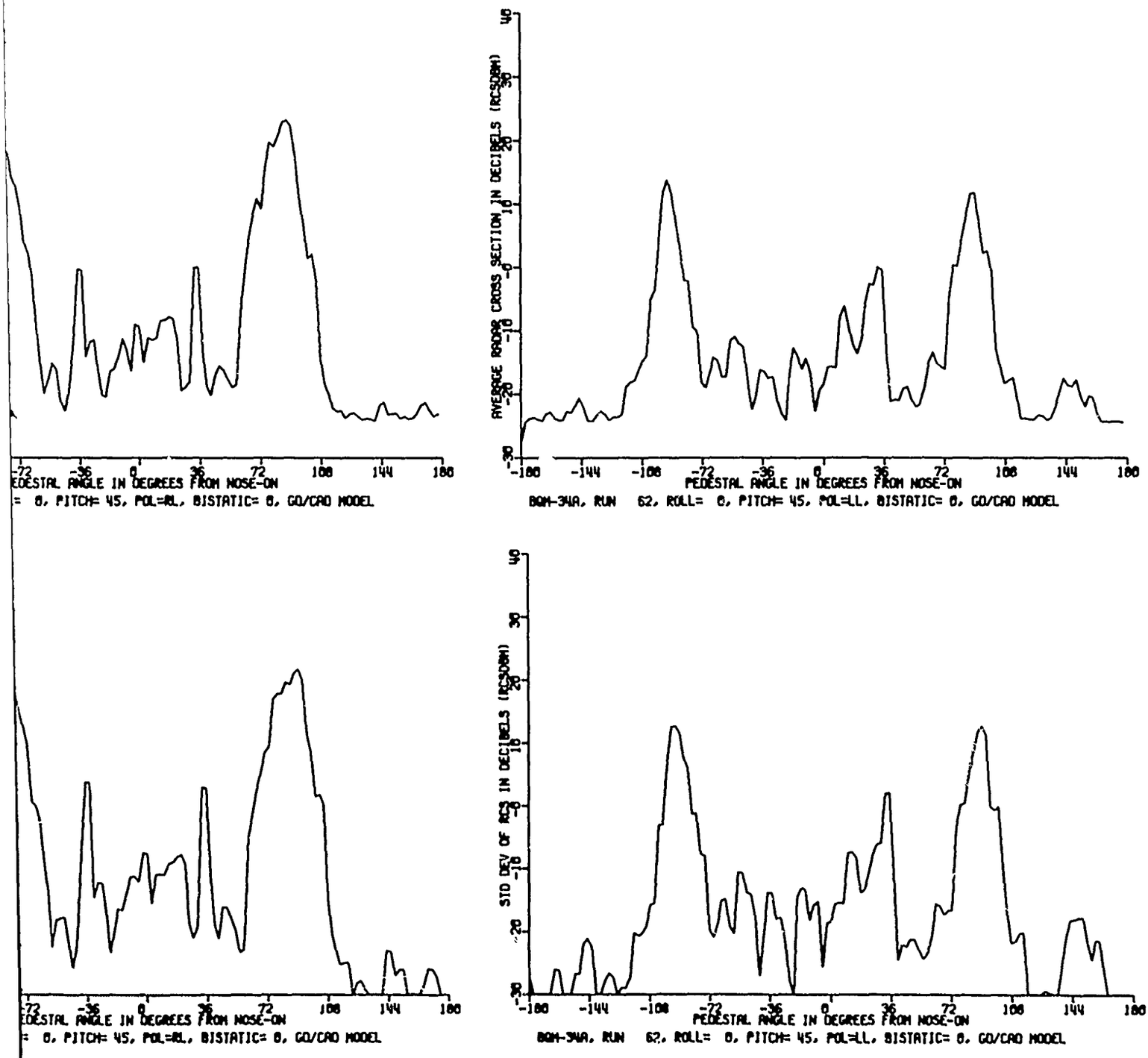

Figure 13. Average and standard deviation of measured RCS, 45° pitch, 0° roll.

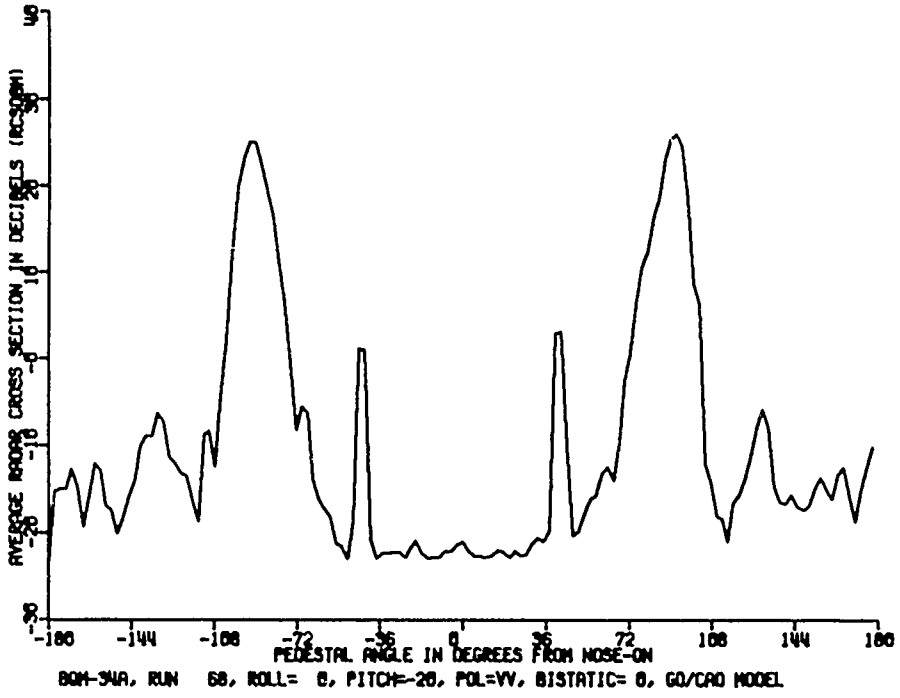

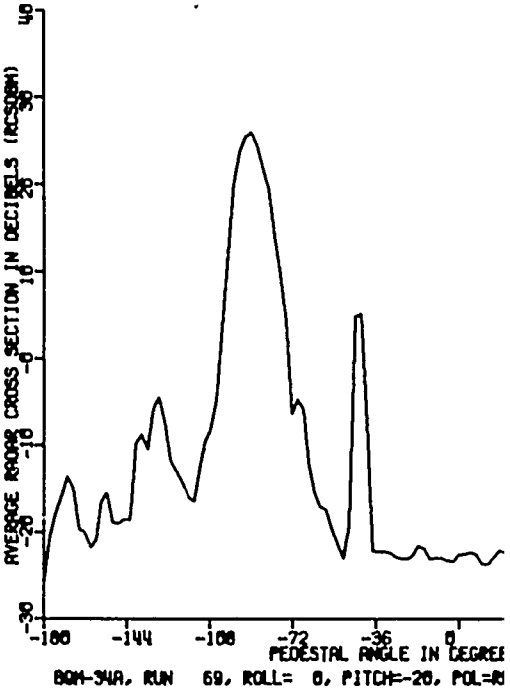

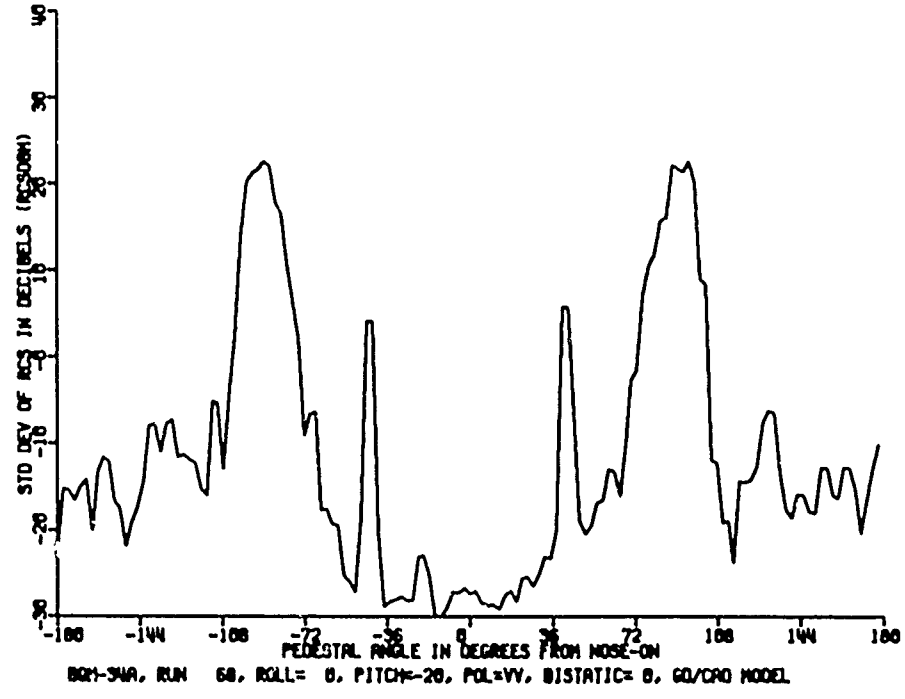

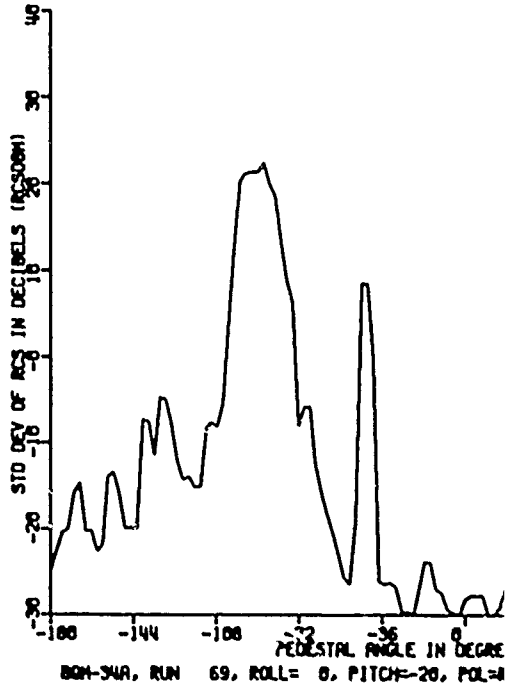

Figure 14. Average and standard deviation of measured RCS, 20° pitch, 0° roll.

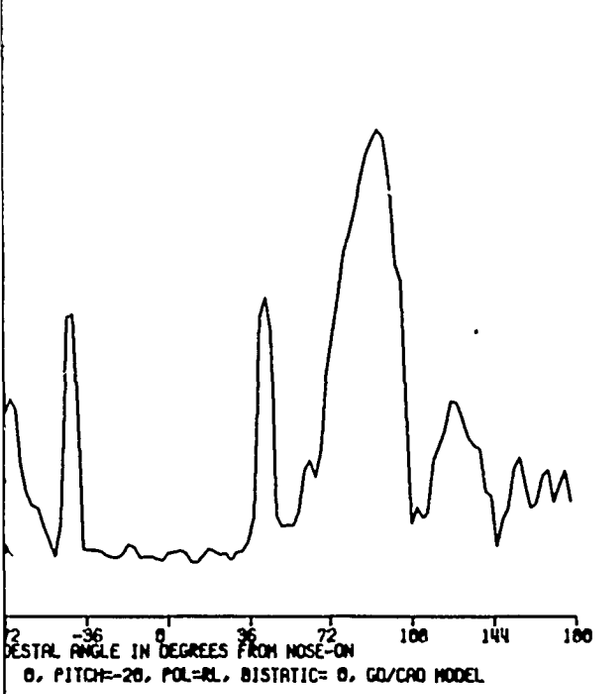
-72 -36 0 36 72 108 144 180
DESTAL ANGLE IN DEGREES FROM NOSE-ON
0, PITCH=-20, POL=RL, BISTATIC= 0, GO/CAO MODEL

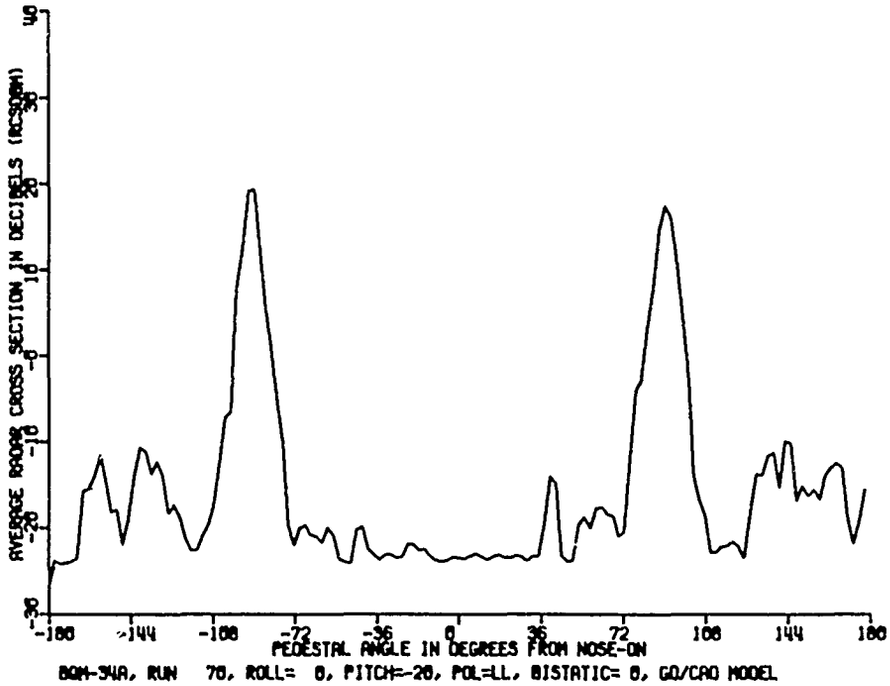
AVERAGE RADAR CROSS SECTION IN DECIBELS (RCSDBM)
40
30
20
10
0
-10
-20
-30
-180 -144 -108 -72 -36 0 36 72 108 144 180
PEDESTAL ANGLE IN DEGREES FROM NOSE-ON
BQM-34A, RUN 70, ROLL= 0, PITCH=-20, POL=LL, BISTATIC= 0, GO/CAO MODEL

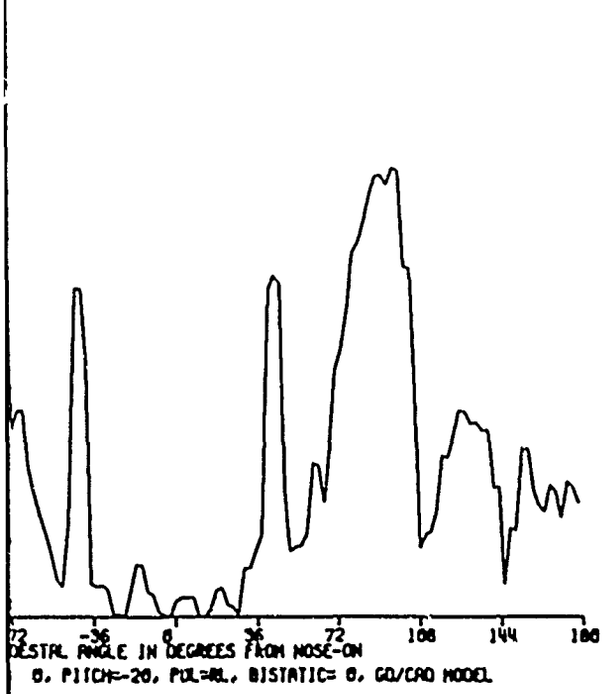
-72 -36 0 36 72 108 144 180
DESTAL ANGLE IN DEGREES FROM NOSE-ON
0, PITCH=-20, POL=RL, BISTATIC= 0, GO/CAO MODEL

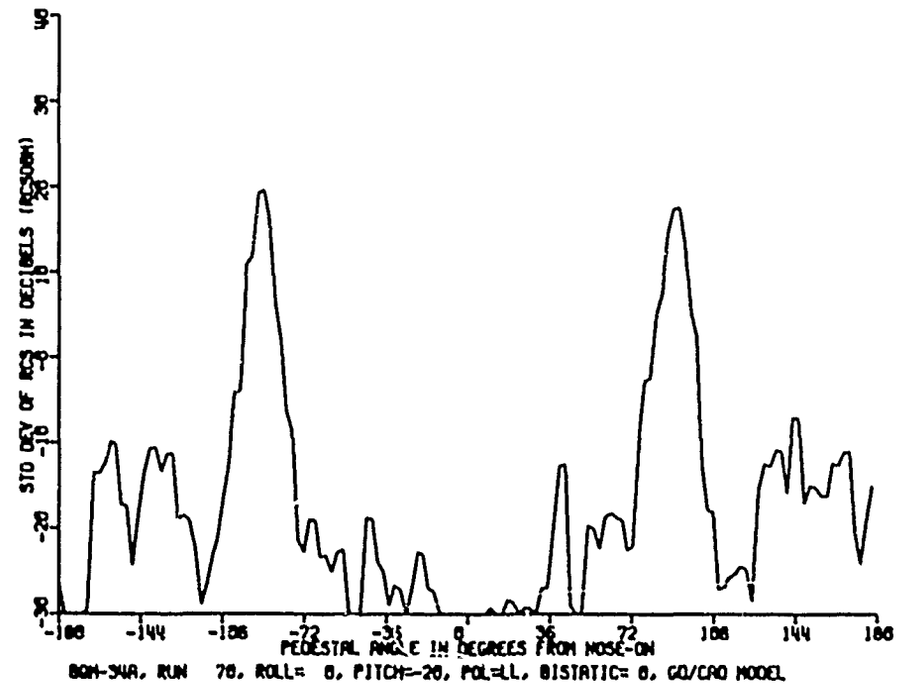
STD DEV OF RCS IN DECIBELS (RCSDBM)
40
30
20
10
0
-10
-20
-30
-180 -144 -108 -72 -36 0 36 72 108 144 180
PEDESTAL ANGLE IN DEGREES FROM NOSE-ON
BQM-34A, RUN 70, ROLL= 0, PITCH=-20, POL=LL, BISTATIC= 0, GO/CAO MODEL

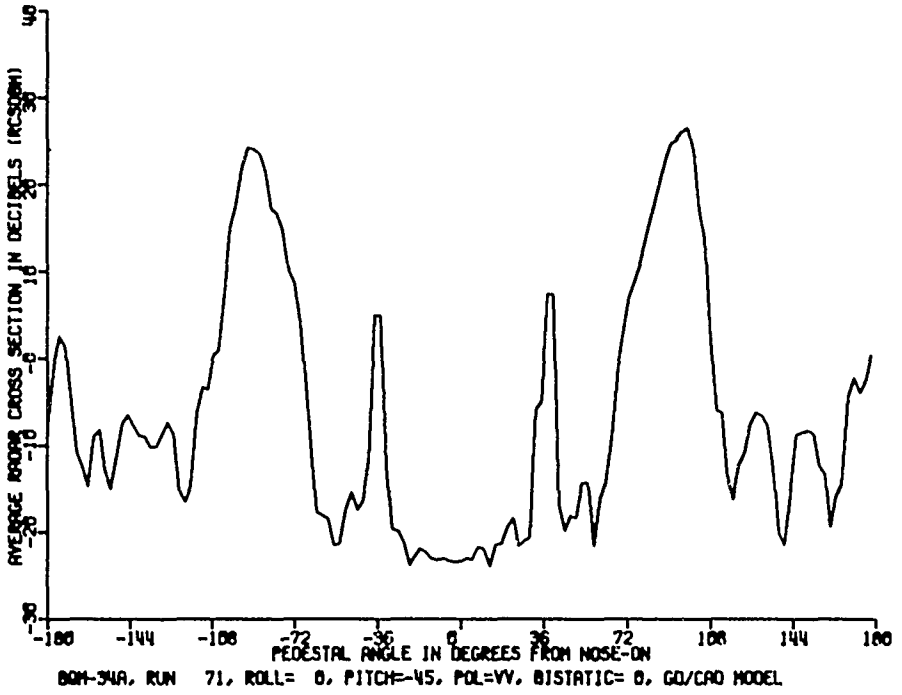

BQM-34A, RUN 71, ROLL= 0, PITCH=-45, POL=VV, BISTATIC= 0, GO/CFO MODEL

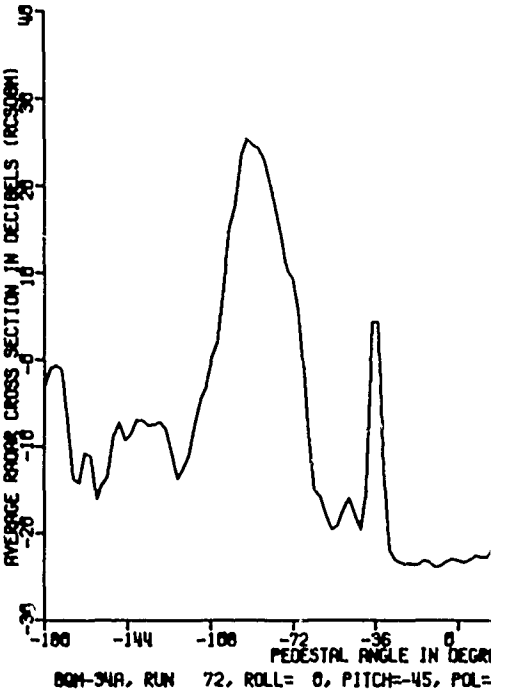

BQM-34A, RUN 72, ROLL= 0, PITCH=-45, POL=

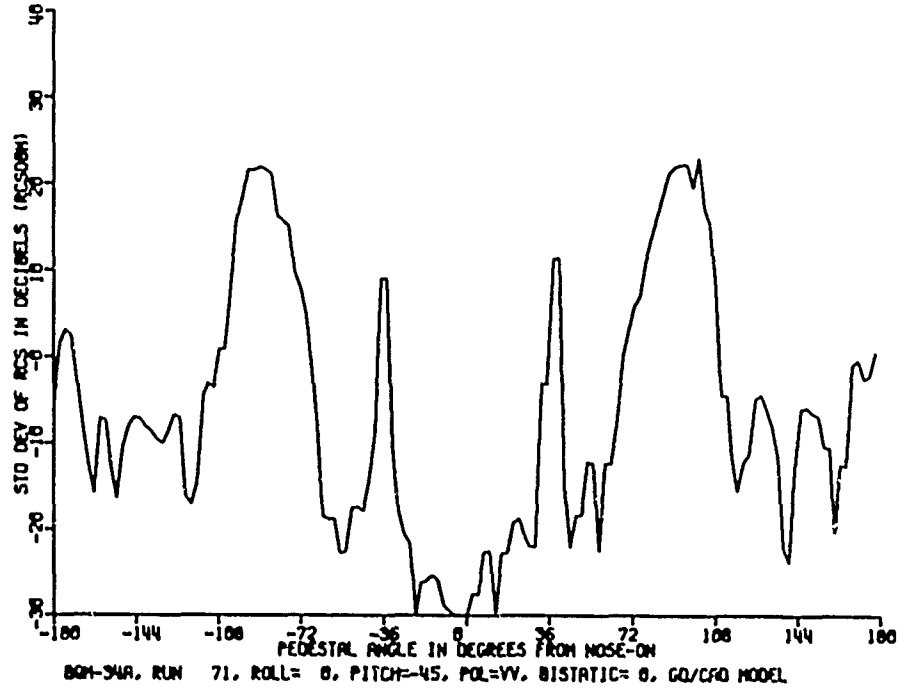

BQM-34A, RUN 71, ROLL= 0, PITCH=-45, POL=VV, BISTATIC= 0, GO/CFO MODEL

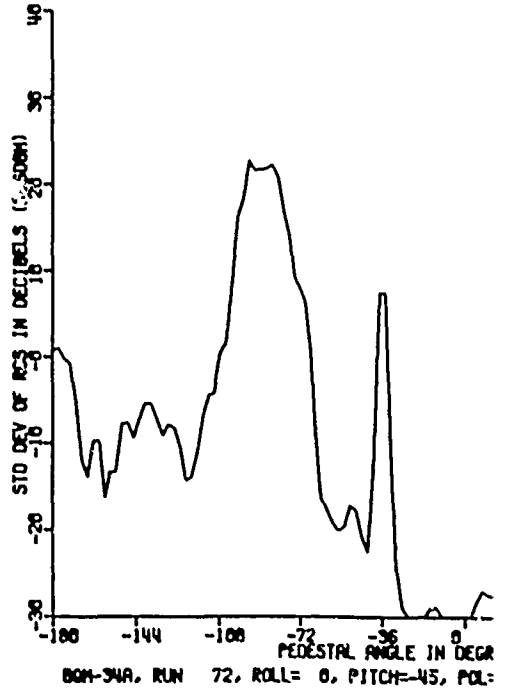

BQM-34A, RUN 72, ROLL= 0, PITCH=-45, POL=

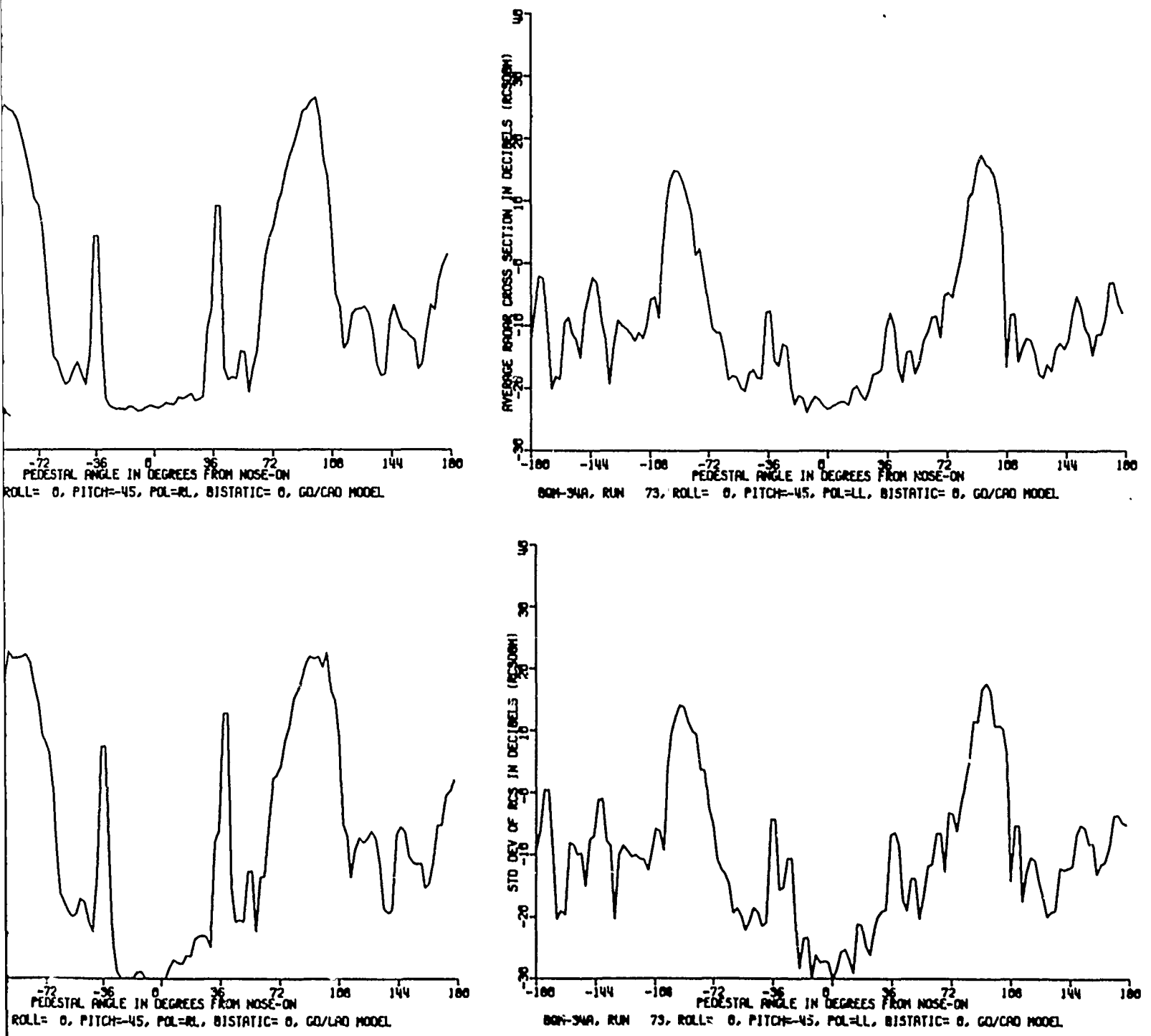

Figure 15. Average and standard deviation of measured RCS, -45° pitch, 0° roll.

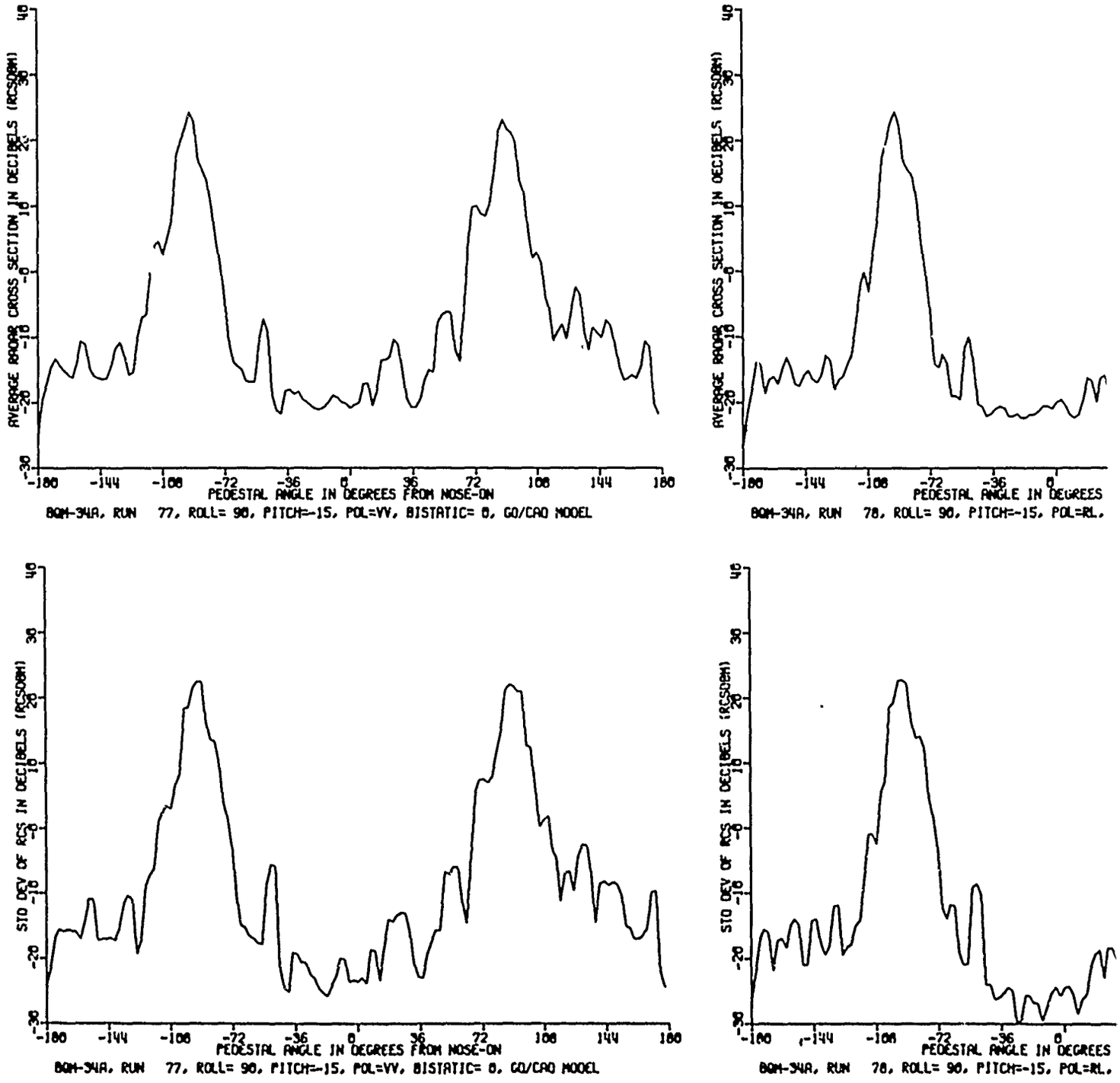

Figure 16. Average and standard deviation of measured RCS, -15° pitch, 90° roll.

ITCH=-15, POL=RL, BISTATIC= 0, GO/CAO MODEL

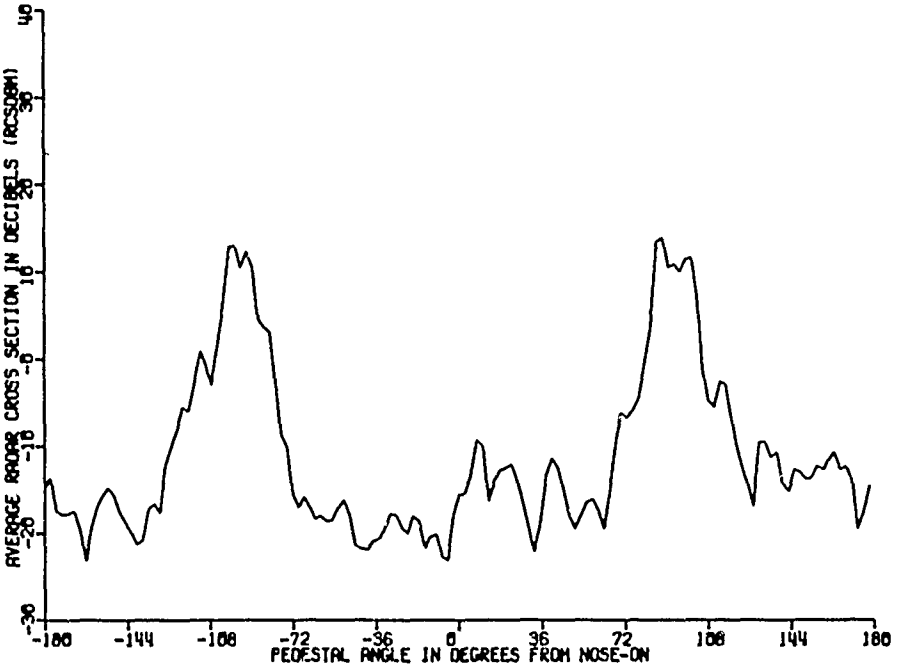

BQM-34A, RUN 79, ROLL= 90, PITCH=-15, POL=LL, BISTATIC= 0, GO/CAO MODEL

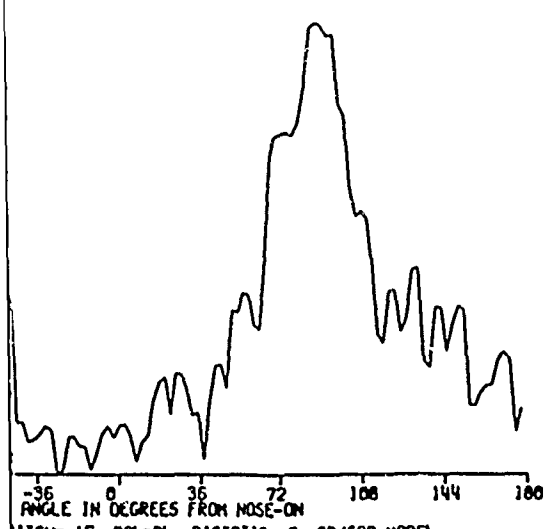

ITCH=-15, POL=RL, BISTATIC= 0, GO/CAO MODEL

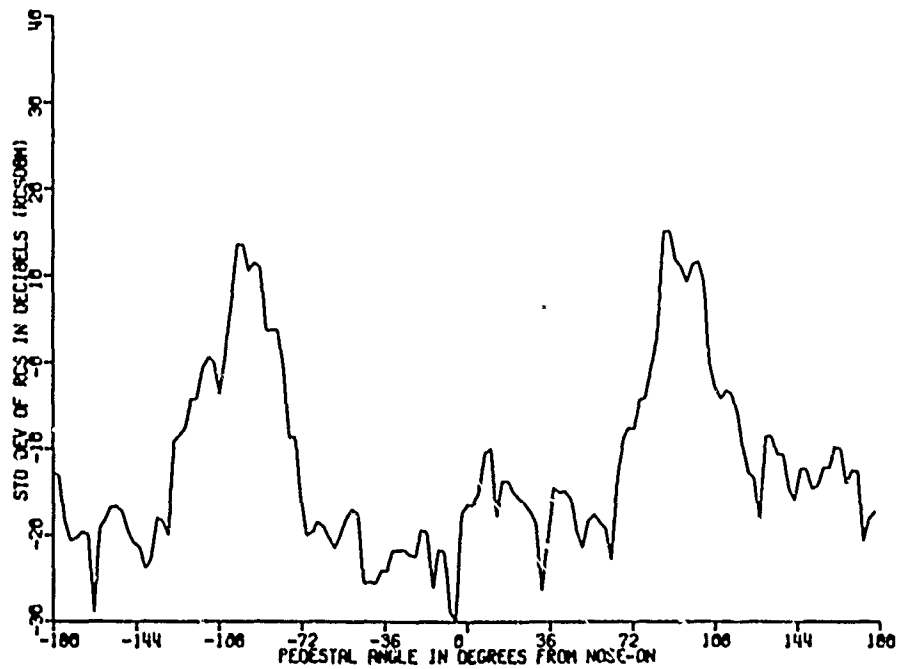

BQM-34A, RUN 79, ROLL= 90, PITCH=-15, POL=LL, BISTATIC= 0, GO/CAO MODEL

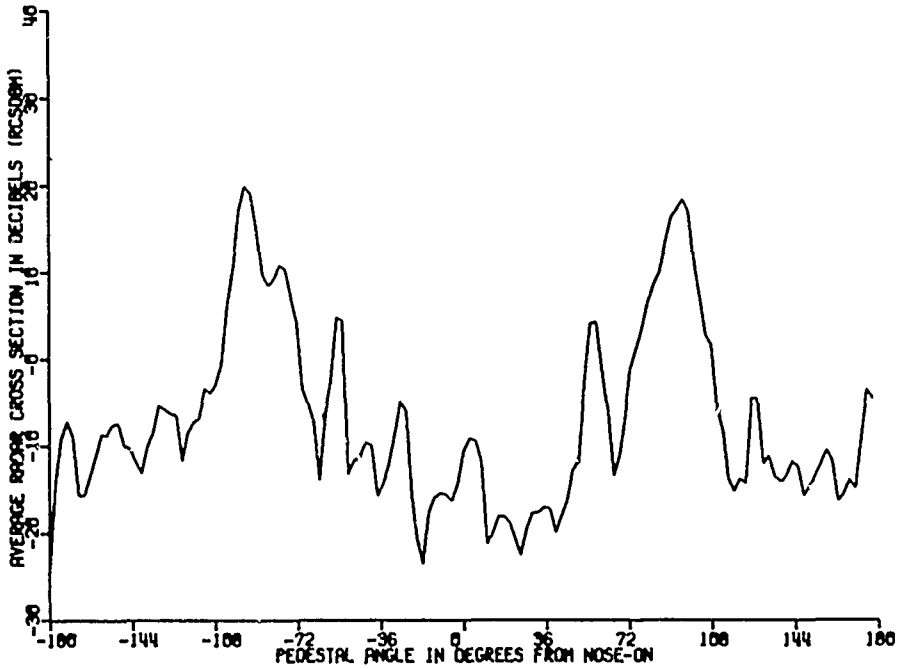

BQM-34A, RUN 80, ROLL= 45, PITCH= 0, POL=VV, BISTATIC= 0, GO/CAO MODEL

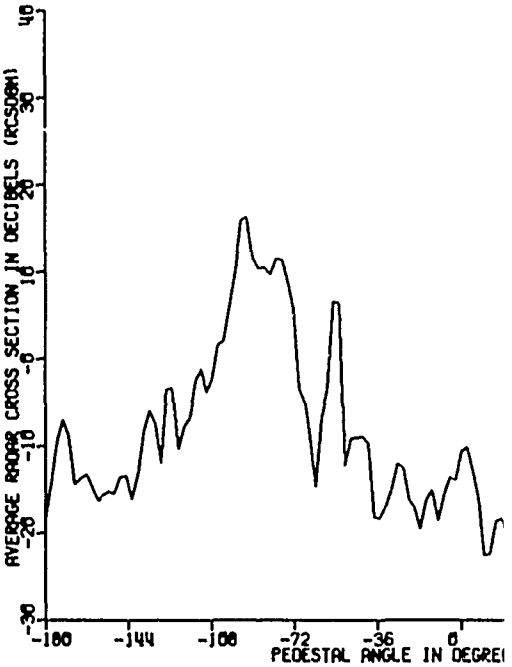

BQM-34A, RUN 81, ROLL= 45, PITCH= 0, POL=R

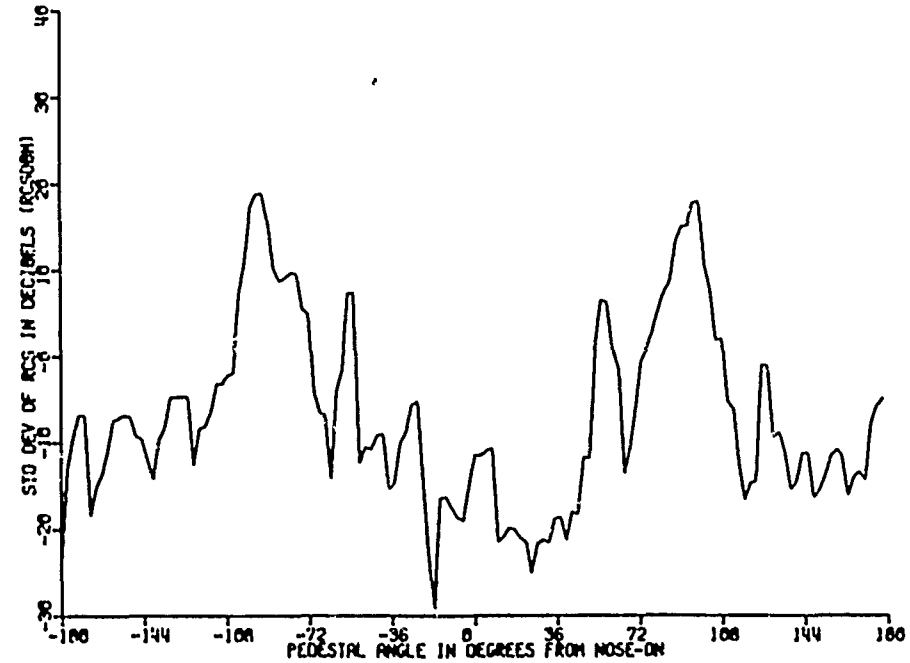

BQM-34A, RUN 80, ROLL= 45, PITCH= 0, POL=VV, BISTATIC= 0, GO/CAO MODEL

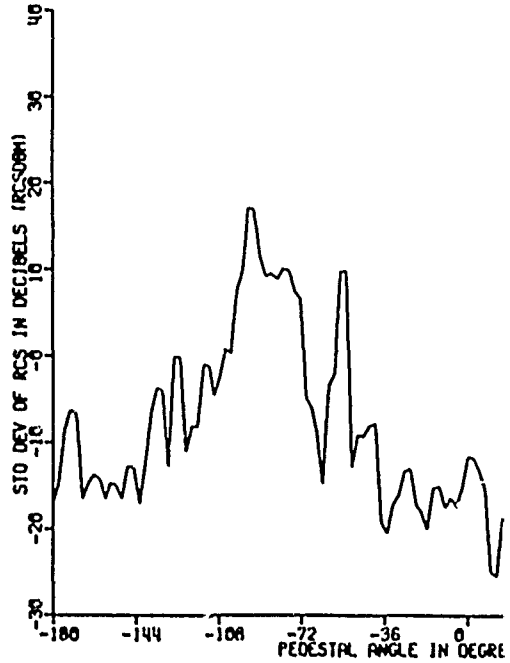

BQM-34A, RUN 81, ROLL= 45, PITCH= 0, POL=

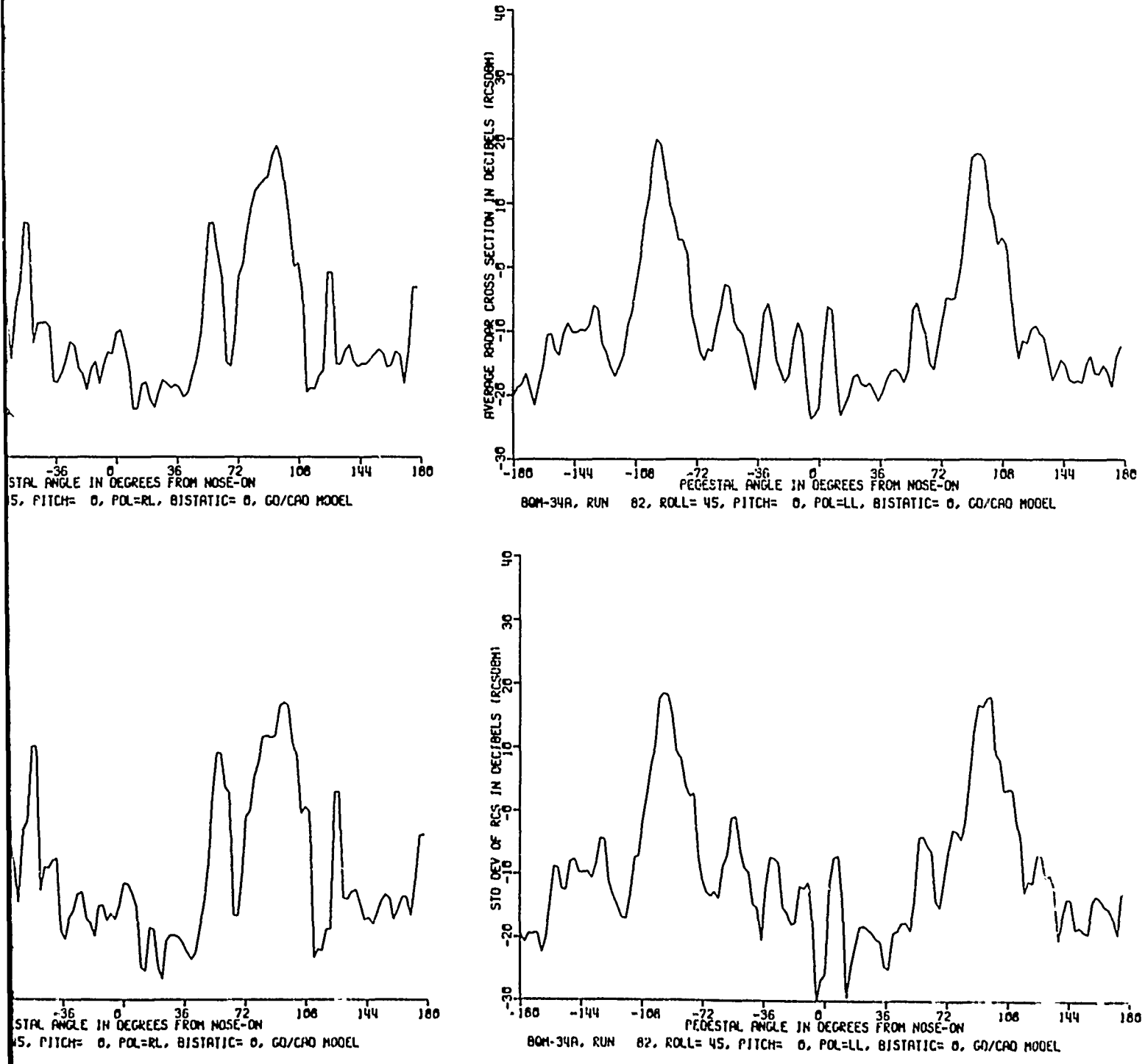

Figure 17. Average and standard deviation of measured RCS, 0° pitch, 45° roll.

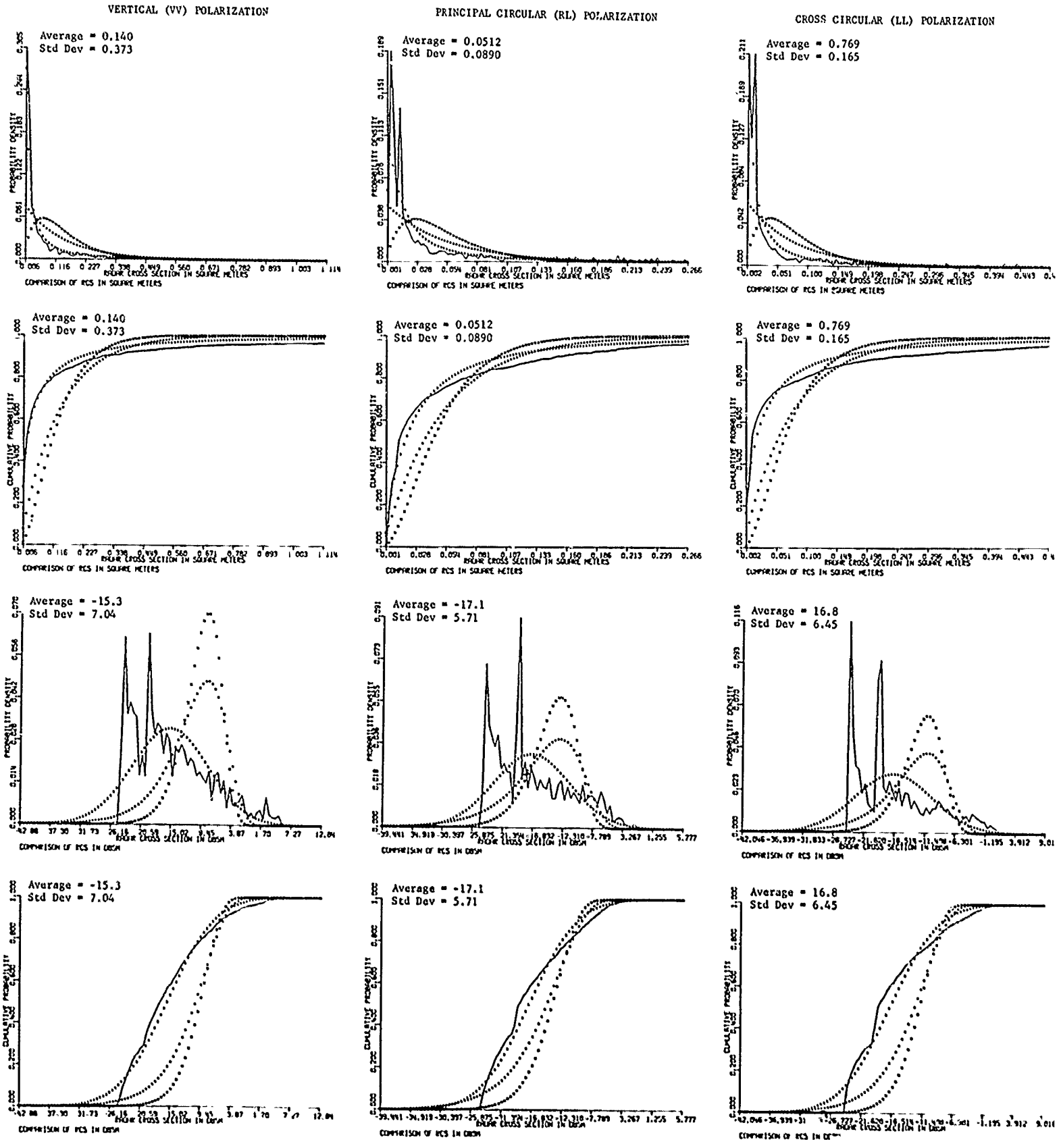

Figure 18. Comparison of measured data and theoretical models for aspect angles within 15° of nose-on.

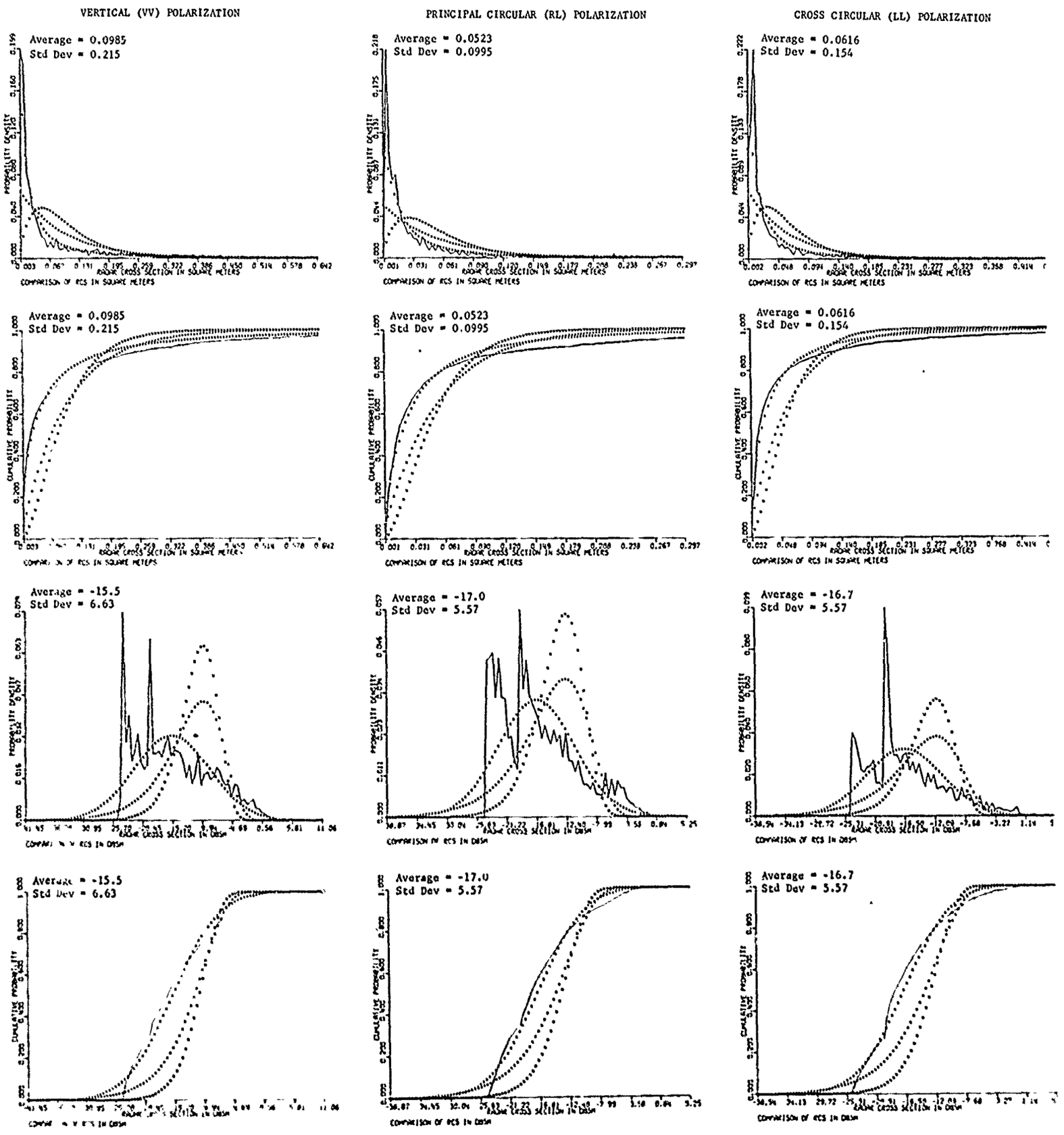

Figure 19. Comparison of measured data and theoretical models for aspect angles greater than 15° and less than 30° from nose-on.

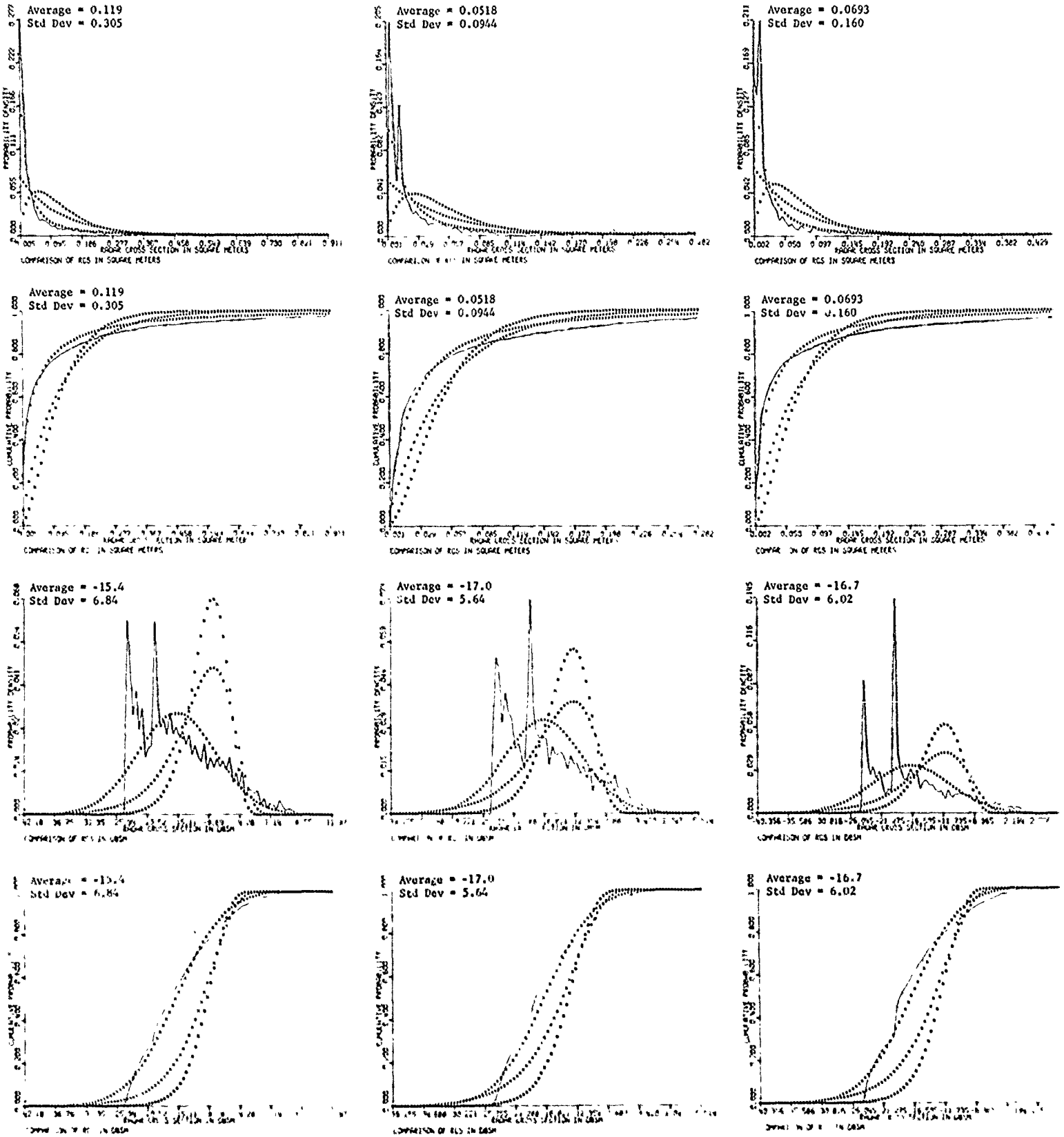

Figure 20. Comparison of measured data and theoretical models for aspect angles within 30° from nose-on.

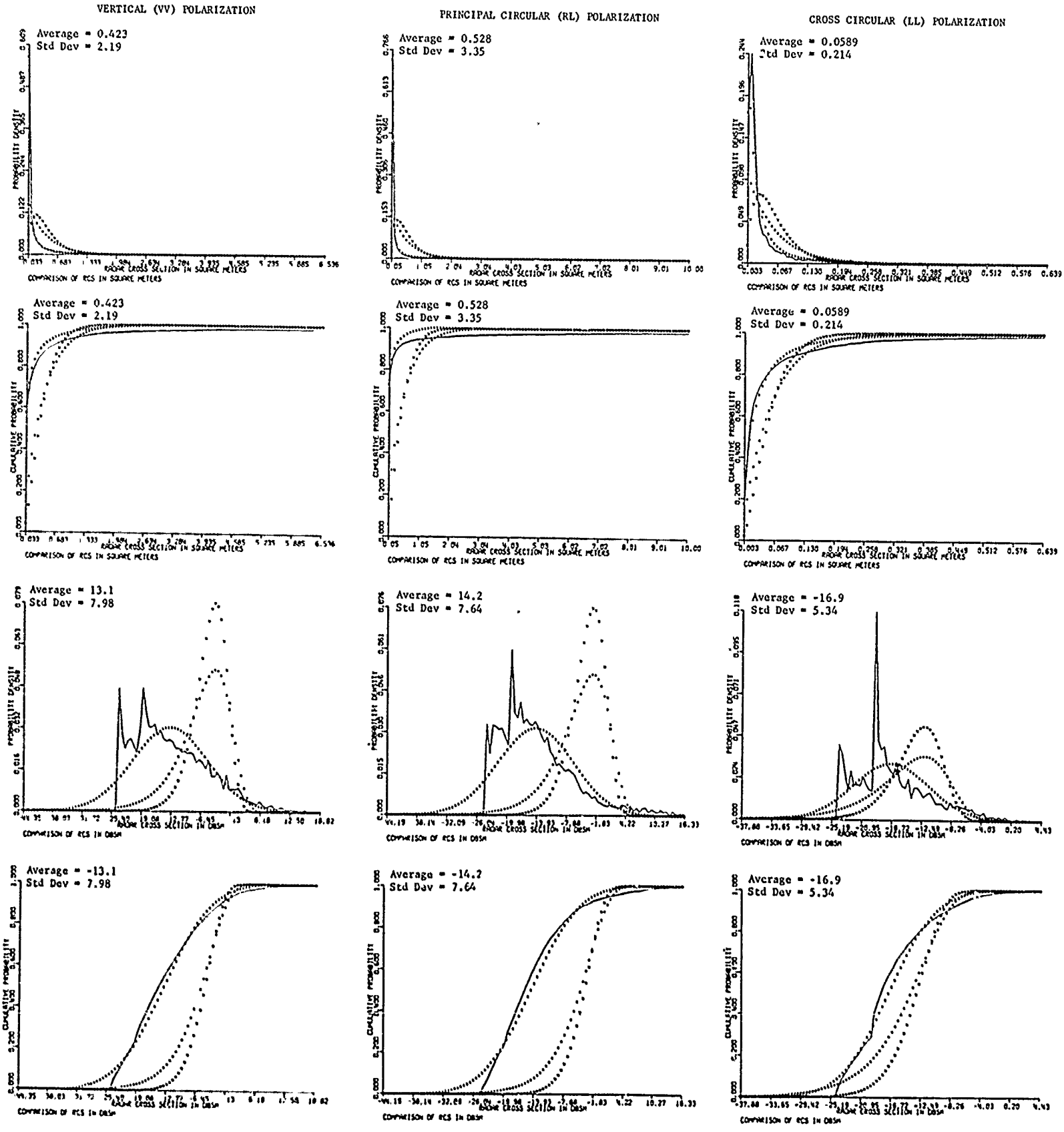

Figure 21. Comparison of measured data and theoretical models for aspect angles greater than 30° and less than 60° from nose-on.

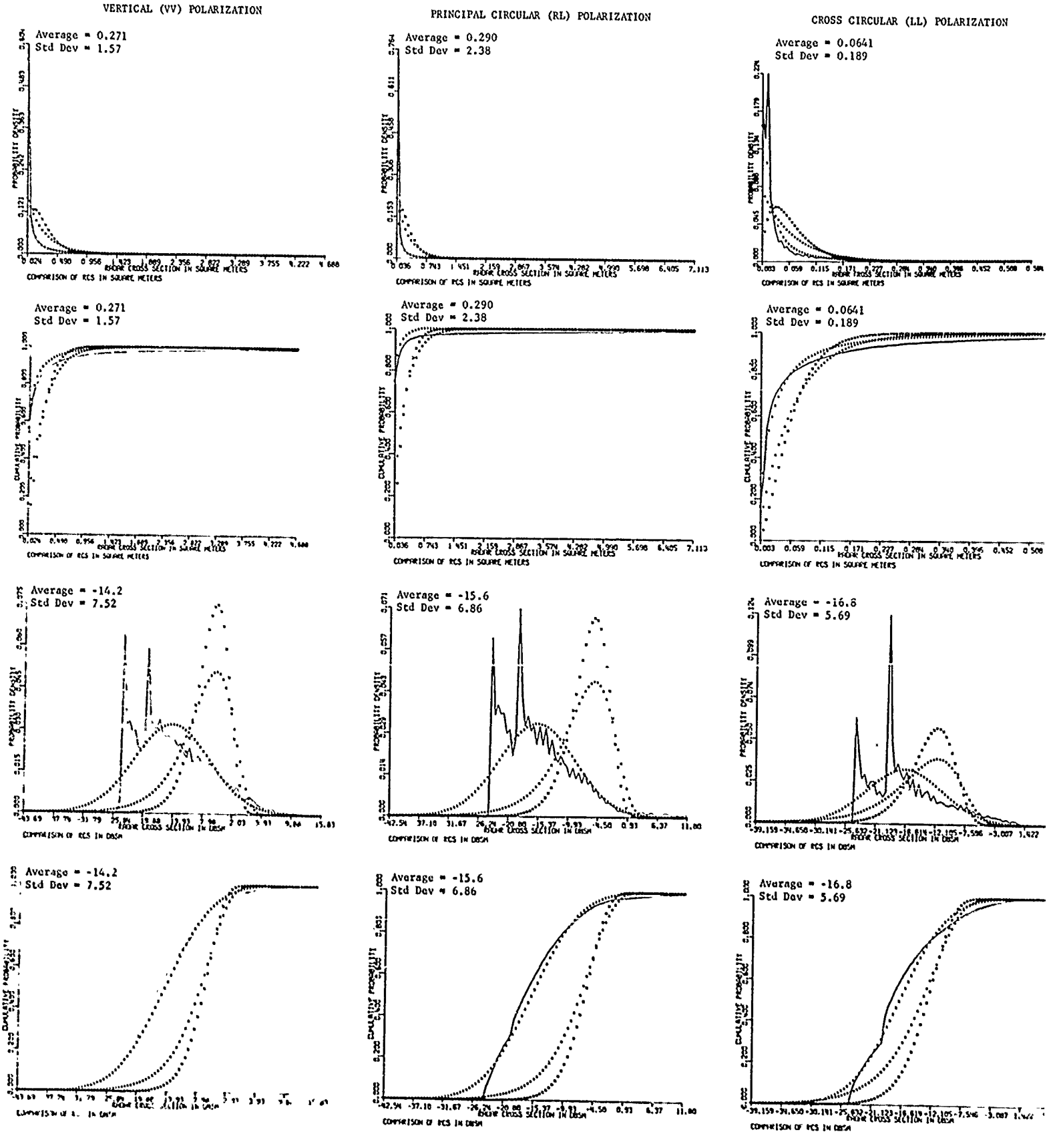

Figure 22. Comparison of measured data and theoretical models for aspect angles within 60° of nose-on.

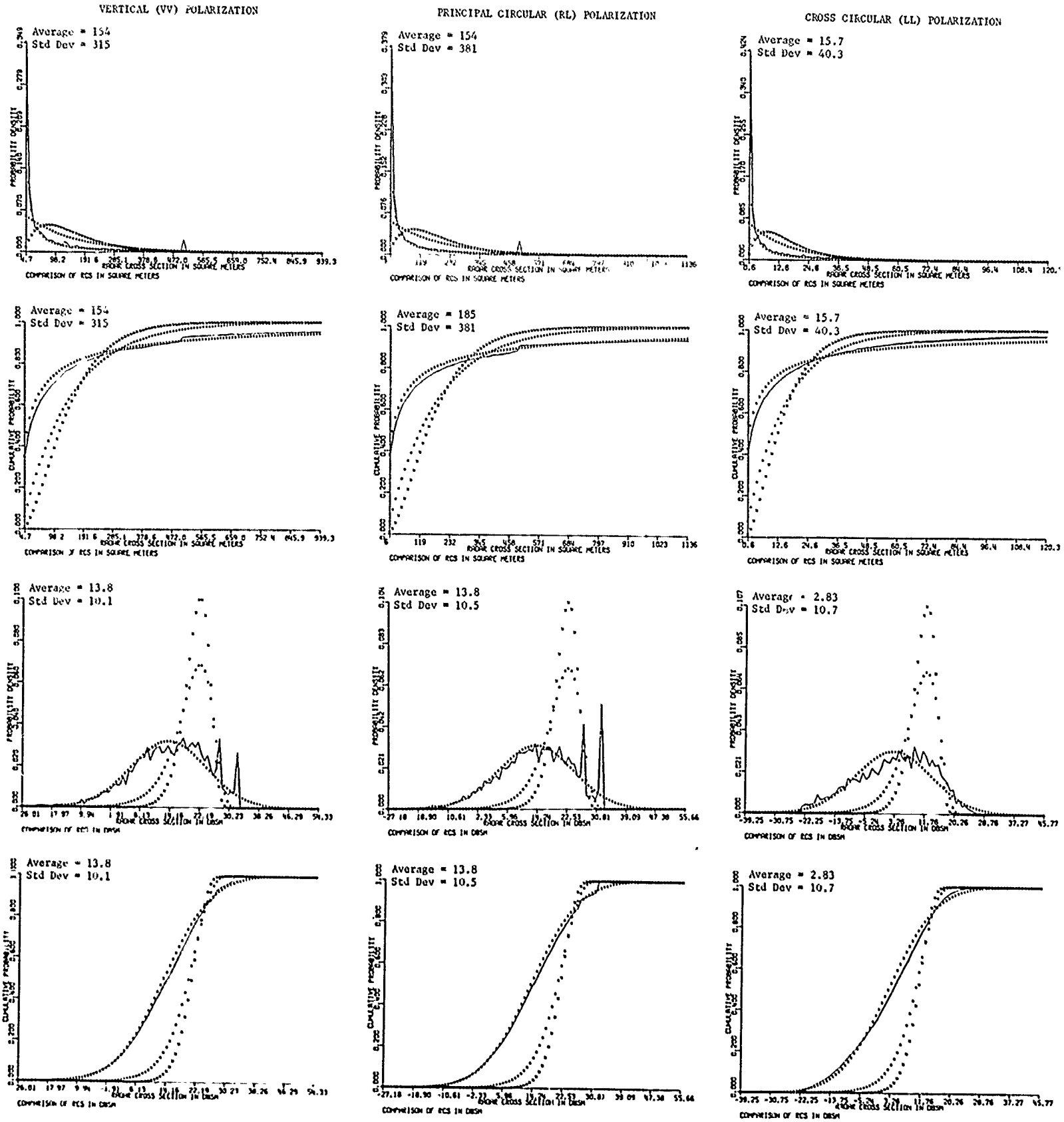

Figure 23. Comparison of measured data and theoretical models for aspect angles within 15° of normal to the roll axis.

DISTRIBUTION

	No. of Copies
Defense Documentation Center Cameron Station Alexandria, Virginia 22314	12
Commander US Army Materiel Command ATTN: AMCRD-WM, Mr. Sedlak AMCRD 5001 Eisenhower Avenue Alexandria, Virginia 22333	1 1
Air Force Avionics Laboratory (WRP) Air Force Systems Command Wright-Patterson AFB, Ohio 45433	1
US Air Force Armament Laboratory (DLMQ) Eglin Air Force Base, Florida 32542	2
Naval Missile Center ATTN: Code 5311 Point Mugu, California 93042	1
Naval Weapons Center ATTN: Code 3911 China Lake, California 93555	1
US Air Force 658 5th Test Group (RX) Holloman AFB, New Mexico 88330	1
Teledyne-Micronetics 7155 Mission Gorge Road San Diego, California 92120	1
Teledyne-Ryan ATTN: Mr. Frank Marshall 2701 Harbor Drive San Diego, California 92112	1
University of Illinois Electromagnetics Laboratory ATTN: Dr. R. Mittra Urbana, Illinois 61801	1

	No. of Copies
General Dynamics Convair Aerospace Division ATTN: Mr. Larry Langston P.O. Box 748 Fort Worth, Texas 76101	1
Westinghouse Electric Corporation Systems Development Division ATTN: Dr. A. F. Gaheen P.O. Box 746 Baltimore, Maryland 21203	1
Raytheon Company Missile Systems Division ATTN: Mr. M. Sisle Hartwell Road, Massachusetts 01730	1
Motorola Government Electronics Division ATTN: Mr. W. Swindell 8201 East McDowell Road Scottsdale, Arizona 85252	1
Calspan Corporation P. O. Box 235 Buffalo, New York 14221	1
AMCPM-MD	1
-MDT	1
-MDE	1
-HAE	1
-HAQ	1
AMSMI-FR, Mr. Strickland	1
-LP, Mr. Voigt	1
-R, Dr. McDaniel	1
Dr. Kobler	1
-RBD	3
-RE, Mr. Lindberg	1
Mr. Pittman	1
-RER	25
-RPR (Record Set)	1
(Reference Copy)	1